

This work was written as part of one of the author's official duties as an Employee of the United States Government and is therefore a work of the United States Government. In accordance with 17 U.S.C. 105, no copyright protection is available for such works under U.S. Law.

Public Domain Mark 1.0

<https://creativecommons.org/publicdomain/mark/1.0/>

Access to this work was provided by the University of Maryland, Baltimore County (UMBC) ScholarWorks@UMBC digital repository on the Maryland Shared Open Access (MD-SOAR) platform.

**Please provide feedback**

Please support the ScholarWorks@UMBC repository by emailing [scholarworks-group@umbc.edu](mailto:scholarworks-group@umbc.edu) and telling us what having access to this work means to you and why it's important to you. Thank you.

# Impacts of Unsteady Flow Environments on the Propulsive Performance of Oscillating Foils

Naresh Poudel<sup>\*</sup> and Meilin Yu<sup>†</sup>

*University of Maryland Baltimore County, Baltimore, MD, 21250, USA*

John T. Hrynuk<sup>‡</sup>

*DEVCOM – Army Research Lab, Aberdeen Proving Ground, MD, 21005, USA*

A numerical study is conducted to understand the impact of an unsteady freestream on the aerodynamic performance of an oscillating airfoil. The unsteady flow environment is generated by placing a stationary inline circular cylinder array upstream of the oscillating airfoil. The dependence of thrust with variation of Reynolds numbers and Strouhal numbers is investigated, and it is revealed that the unsteady flow environment enhances thrust production of a pitching airfoil. This increased thrust production was related to an effective increase in the Reynolds number experienced by the airfoil. With airfoil-vortex interaction analysis, the increase in average thrust coefficient was shown to be caused by constructive interaction of freestream vortex structures and the oscillating airfoil. Drag inducing interactions were also observed but were less common than thrust increasing events, resulting in a higher average thrust. A simple scaling law is expanded to include the effects of unsteadiness, where thrust is found to be linearly dependent on turbulence intensity. It is demonstrated that the thrust generated by the pitching airfoil when operating in highly unsteady flow environments is more accurately represented as a function of Reynolds number, Strouhal number, and turbulence intensity.

## Nomenclature

$A$	=	planform area, $[m^2]$
$A_{pitch}$	=	pitching amplitude, $[m]$
$C_D$	=	offset drag
$C_p$	=	pressure coefficient; $\frac{p - p_\infty}{\rho U_\infty^2 / 2}$
$C_T$	=	thrust coefficient; $\frac{-F_x}{\rho U_\infty^2 A / 2}$
$\overline{C_T}$	=	time-averaged thrust coefficient
$c$	=	chord length of airfoil, $[m]$

---

<sup>\*</sup>Graduate Student, Department of Mechanical Engineering, npoudel1@umbc.edu, and AIAA Student Member.

<sup>†</sup>Associate Professor, Department of Mechanical Engineering, mlyu@umbc.edu, and AIAA Senior Member.

<sup>‡</sup>Mechanical Research Engineer, Weapons and Materials Research Directorate, DEVCOM Army Research Lab

$d$	=	cylinder diameter, $[m]$
$dt$	=	time step
$f$	=	pitching frequency, $[s^{-1}]$
$F_x$	=	force in x-direction, $[N]$
$k$	=	reduced frequency; $\frac{\pi f c}{U_\infty}$
$p$	=	pressure, $[Pa]$
$p_\infty$	=	freestream pressure, $[Pa]$
$Re$	=	Reynolds number based on airfoil chord; $U_\infty c / \nu$
$\widetilde{Re}$	=	effective Reynolds number
$St$	=	Strouhal number; $\frac{2fA_{pitch}}{U_\infty}$
TG	=	turbulence generator
$TI$	=	turbulence intensity; $u' / \bar{u}$
$t$	=	dimensional time, $[s]$
$t^*$	=	non-dimensional time; $tU_\infty / c$
$U_\infty$	=	freestream velocity, $[m/s]$
$\bar{u}$	=	mean of the streamwise velocity, $[m/s]$
$u'$	=	root mean square of the streamwise velocity, $[m/s]$
$\beta$	=	coefficient of thrust scaling
$\theta$	=	pitching angle amplitude, $[degree]$
$\phi$	=	initial phase
$\rho$	=	density, $[kg/m^3]$
$\nu$	=	kinematic viscosity, $[m^2/s]$

## I. Introduction

THE presence of an unsteady and highly turbulent environment for small- and mid-scale unmanned aerial vehicles (UAVs) in real-world conditions suggests that unsteady freestream conditions may have a significant impact on their performance. As a matter of fact, flying insects, birds, and swimming fish are known to encounter a highly dynamic and unsteady environment and have been observed to use external flow disturbances to reduce the cost of locomotion [1–4]. Wu *et al.* [5] have recently presented a thorough overview of the current state of bio-inspired flapping foils research. They concluded that the majority of research in this area has focused on single foils in steady flow conditions at low or moderate Reynolds numbers, and recommended that future research should move towards flow behaviors more closely associated with real-world situations, such as three-dimensionality, the introduction of freestream turbulence,

and investigations at a wider variety of Reynolds numbers. As noted by Wu *et al.* [5], at low Reynolds numbers considerable research has also been conducted to investigate the influence of Reynolds number on propulsive efficiency [6–11]. In general these studies observed that increasing the Reynolds number reduces drag, resulting in net positive thrust. Senturk and Smits [10] reported that thrust and power are relatively insensitive to Reynolds number when Reynolds number is greater than about 16,000 in their study. At high Reynolds numbers, e.g.,  $Re = 10^6$ , Catlett *et al.* [12] showed that reduced frequency was a critical factor in the flow behavior and that the unsteady forces could be adequately modeled with potential flow theory. However, these studies have generally focused on uniform flow conditions when determining the propulsive performance of oscillating wings.

In nature turbulence intensity or unsteadiness has been observed to be as high as 30% in suburban areas near the atmospheric boundary and up to 50% near high-rise structures [13–15]. Similarly, vegetation, dead wood, pipelines, and bridge piers generate turbulence and sometimes even coherent, periodic flow structures in which fish swim [16]. Significant biologic system focused research has been conducted on the effects of freestream unsteadiness such as turbulence on flying insects, birds, and fish [17–25]. We briefly review previous studies on fish and fishlike swimming in an unsteady environment here as this has inspired our current research on studying the impact of flow environment unsteadiness on the propulsive performance of flapping foils. We note that fish and fishlike swimming in unsteady environments have been extensively studied experimentally [4, 26–28] and numerically [29–32] to investigate potential benefits of the unsteady incoming flow. Upstream objects such as circular cylinders or D-section cylinders are used in these studies to characterize the flapping foil based propulsive performance. Liao *et al.* [4, 27, 28] observed rainbow trout synchronising their body kinematics with flow disturbances to reduce the power required for propulsion. Akanyeti and Liao [33] proposed a Kármán gait analytical model that fully describes rainbow trout responses to vortex street based on the experiments. Shao *et al.* [31] numerically studied the interaction between a flapping airfoil in the wake of an oscillating half-cylinder. They observed that for some wake modes the strong interaction of the incoming vortices with the airfoil induced low pressure at the leading edge, resulting in a larger thrust. However in other cases the interaction with the incoming vortices is weak, and the thrust is increased only slightly. We mention that these previous studies focused on the impact of structured vortex environment on the performance of flapping wing/fin based propulsion. Considerably less work has been done to characterize the impact of random, turbulent flow environments on flapping wing/fin propulsive performance. We now briefly review relevant studies along this research route.

The influence of freestream turbulence on static stall of airfoils has also been widely investigated [34–38]. Increased turbulence in the freestream has been shown to raise the maximum lift coefficient and delays flow separation, hence postponing stall. Hoffmann [34] performed an experimental study on a NACA0015 airfoil and found that increasing the turbulence intensity from 0.25% to 9.0% delayed flow separation and increased the maximum lift by up to 30%. Similarly, Devinant *et al.* [35], Amandolé and Széchényi [39], and Sicot *et al.* [36] also showed that increasing the turbulence intensity increased maximum lift in their experiments. However, cambered airfoils may have a lower

maximum lift coefficient in increased turbulence. Kay *et al.* [38] evaluated NACA 0012 and NACA 4412 airfoils at moderate Reynolds numbers (50,000–200,000) with turbulence intensities varying from 1.3 to 15%. When turbulence intensity was increased the cambered airfoil's maximum lift coefficient decreased by up to 30%, while lift on the symmetrical NACA 0012 airfoil increased by 5%. Wang *et al.* [37] similarly studied the NACA 0012 airfoil at Reynolds numbers ranging from  $5.3 \times 10^3$  to  $2.0 \times 10^4$  and turbulence intensities of 0.6% and 6.0%. They observed that at low Reynolds numbers, increasing turbulence intensity had a similar effect on the airfoil wake as increasing the Reynolds number. They documented that increasing turbulence intensity or Reynolds number both served to trigger shear layer transition and reattachment, sometimes forming a separation bubble. They also introduced the concept of an effective Reynolds number, which considered the turbulence intensity effect as that from an increased Reynolds number, albeit the two effects are not exactly identical. Recently, a few studies [40, 41] investigated static wing performance in an unsteady freestream generated by placing an object upstream of the wing. They discovered that the stall was delayed due to the influence of the upstream cylinder, similar to other turbulence studies.

More work has been done in the area of dynamic stall in unsteady environments, using oscillating inflow velocity conditions [42–45], turbulence grids [39, 46, 47] and upstream cylinders to create disturbances [48, 49]. In the presence of freestream turbulence, these studies demonstrated a delay in boundary layer separation and a smaller separation bubble over the maneuver's surface. When the turbulence intensity is increased, the dynamic stall process is delayed to higher incidence angles [50]. Gharali and Johnson [45] conducted a two-dimensional (2D) numerical study of a pitching airfoil with the unsteady inflow velocity to investigate the velocity phase difference between the freestream velocity oscillation and the pitching pattern oscillation, similar to Favier's experiment [42]. This work indicated that for in-phase oscillations, the lift could be about 5 times greater than that in the static freestream and this value could be amplified as the reduced frequency increased. Yu *et al.* [46] used particle-image velocimetry to study dynamic stall in a water tunnel with turbulence intensities of 0.5 and 6.9% at low Reynolds number,  $Re = 4,500$ . They found that higher turbulence intensity (6.9%) delays the dynamic stall event due to a reduction in velocity deficit and flow reversal. Amandolése and Széchényi [39] demonstrated that the lift overshoot hysteresis loop decreased with increasing turbulence. The experimental study by Li *et al.* [47] also discovered that the size of the hysteresis loop caused by dynamic stall gradually decreases with increasing turbulence intensity. Chen and Choa [48] performed an experimental study on the effect of turbulent wakes on a pitching airfoil. In this work, a small cylinder was placed upstream at different vertical positions relative to the pitching airfoil at Reynolds number 80,000 with low reduced frequencies ( $k = 0.01 - 0.04$ ). They compared the aerodynamic forces and moments with those from the undisturbed freestream case, where they observed that dynamic stall occurs at higher angles of attack due to the turbulent wake. The growth of the leading-edge suction peak was also found to be particularly sensitive to the vertical position of the cylinder. Merrill and Peet similarly [49] studied a pitching airfoil in the presence of a turbulent wake produced by an upstream small cylinder. Their study showed that in the presence of upstream wake turbulence the magnitude of drag and pitching

moment were greatly reduced over the majority of the pitching cycle. They also found that dynamic stall starts at a later time and at higher angles of attack due to delayed formation and detachment of the dynamic stall vortex. Conger and Ramaprian [51] investigated a pitching NACA 0015 airfoil in a water channel with a relatively high level of freestream turbulence (0.8–1.0%) compared to other water tunnels. They reported a greater magnitude of pressure forces in their study than was previously reported for similar pitch rates, implying that turbulent effects may extend to dynamic motions of wings. Kay *et al.* [52] demonstrated similar effects as the other studies but at higher Reynolds numbers (50,000–200,000) and higher turbulence intensities (5–15%).

While pioneering studies have shown a variety of turbulent effects on propulsive performance of oscillating wings, it is still not clear how truly unstructured flow features, especially those containing considerable amount of energy, interact with oscillating wings and thus, impact their propulsive performance. The current study aims to bridge this gap by investigating the interaction between a highly unsteady, energy-containing flow environment and an oscillating airfoil. As a first step towards achieving this goal, 2D numerical simulations were conducted in this work to reveal coarse-scale dynamics from the highly nonlinear dynamic system. A key observation is that unstructured flow unsteadiness can consistently enhance thrust production of a pitching airfoil in a wide Reynolds and Strouhal number range. This indicates that unsteady flow environments can save propulsion cost of oscillating airfoils, which shares similarity with the observation from an experimental work on fish swimming in schools [53], stating that in a fish school with unsteady flow environments, individuals in any position have reduced costs of swimming, compared to when they swim at the same speed but alone. We note that “non-uniform” and “unsteady” are used to describe the flow in this study as the 2D numerical simulations conducted have been shown not to produce true three-dimensional (3D) turbulent behaviors [54]. As presented in Section III.A, the created 2D unsteady environment exhibits 2D turbulent features. Nevertheless, we mention that the intrinsic randomness features in the 2D non-uniform flow environment remains similar in principle to those from unsteady environments observed in nature. Furthermore, this work expands on the scaling law first suggested by Senturk and Smits [10] for the uniform flow environment to an unsteady one with turbulence intensity incorporated as a propulsive performance predictor alongside Reynolds number and Strouhal number.

The remainder of the paper is organized as follows. Section II gives a brief overview of the high-order unstructured moving grid based computational fluid dynamics (CFD) solver, as well as the computational setup in this study. The characterization of unsteady flow environments, and verification and validation results are presented in Section III. Numerical results and discussions of the impact of flow unsteadiness on propulsive performance of a pitching airfoil are presented in Section IV. Therein, we also show how flow unsteadiness increases the effective Reynolds number of the flow, and how the thrust scaling law for the uniform flow can be extended to take turbulent effects into consideration. Finally, Section V concludes this study.

## II. Numerical Methods

For completeness, we briefly review the numerical methods and setup in this section. More details regarding the numerical methods can be found in our previous works [55–58].

### A. Governing Equations

Two-dimensional unsteady compressible Navier-Stokes equations in the conservation form, as shown below, are considered in this study:

$$\frac{\partial Q}{\partial t} + \frac{\partial F}{\partial x} + \frac{\partial G}{\partial y} = 0, \quad (1)$$

where  $Q = (\rho, \rho u, \rho v, E)^T$  are conservative variables,  $\rho$  is the density of fluid,  $u$  and  $v$  are the x- and y-components of the velocity vector, and  $E$  is the total energy given by  $E = \frac{p}{\gamma-1} + \frac{1}{2}\rho(u^2 + v^2)$  for a perfect gas in which  $p$  is the pressure and  $\gamma$  is the constant specific heat capacity ratio. The total energy formula closes the solution system.  $F$  and  $G$  are total flux vectors including the inviscid and viscous flux terms in the x- and y-direction, respectively. To facilitate numerical simulation, the governing equation (1) in the physical domain  $(t, x, y)$  is transformed into the computational domain  $(\tau, \xi, \eta)$  as follows:

$$\frac{\partial \tilde{Q}}{\partial \tau} + \frac{\partial \tilde{F}}{\partial \xi} + \frac{\partial \tilde{G}}{\partial \eta} = 0, \quad (2)$$

where

$$\begin{cases} \tilde{Q} = |J|Q, \\ \tilde{F} = |J|(Q\xi_t + F\xi_x + G\xi_y), \\ \tilde{G} = |J|(Q\eta_t + F\eta_x + G\eta_y). \end{cases} \quad (3)$$

Note that in the coordinate transformation,  $\tau = t$  and  $(\xi, \eta) \in [-1, 1] \times [-1, 1]$  is a standard element in the computational domain. In Eq. (3),  $J$  is the Jacobian matrix of the coordinate transformation, and  $\xi_t, \xi_x, \xi_y, \eta_t, \eta_x$  and  $\eta_y$  are corresponding metrics of the coordinate transformation.  $\xi_t$  and  $\eta_t$  are related to the grid velocity vector  $\vec{v}_{grid}$  as

$$\begin{cases} \xi_t = -\vec{v}_{grid} \cdot \nabla \xi, \\ \eta_t = -\vec{v}_{grid} \cdot \nabla \eta. \end{cases} \quad (4)$$

The geometric conservation law (GCL) has been enforced following the error compensation approach by Yu *et al.* [59].

### B. Spatial Discretization and Time Integration Methods

The high-order flux reconstruction/correction procedure via reconstruction (FR/CPR) method [60, 61] was used to solve the governing equations. In FR/CPR methods, the flux terms in Eq. (2) are divided into two parts, i.e. local fluxes  $\tilde{F}^{loc}$  constructed from local solutions and correction fluxes  $\tilde{F}^{cor}$  by mapping the differences between the local

fluxes and the common fluxes on the element interfaces into the entire element with high-order correction functions. In this study, the inviscid common fluxes on the element interfaces were calculated using the Roe approximate Riemann solver [62] and the common viscous fluxes were obtained by the second approach (BR2) developed by Bassi and Rebay [63]. The numerical method here utilizes an Implicit Large-Eddy Simulation (ILES) approach [64], where numerical dissipation acts as a sub-grid scale model.

To minimize numerical errors when performing simulations on curved elements [55], Eq. (2) can be transformed back to the physical domain as

$$\frac{\partial Q}{\partial \tau} + \left( \frac{\partial F^{loc}}{\partial \xi} + \frac{\partial G^{loc}}{\partial \eta} \right) + \delta^{cor} - \vec{v}_{grid} \cdot \nabla Q = 0, \quad (5)$$

where  $\delta^{cor}$  is the correction field defined in the FR/CPR method.

Eq. (5) can be further rewritten as

$$\frac{\partial Q}{\partial \tau} = R(Q, \nabla Q), \quad (6)$$

where  $R$  stands for the residual. The linearly implicit Rosenbrock-Wanner (ROW) Runge-Kutta method [65] was used to carry out time integration. In this study, a third-order accurate spatial discretization and a four-stage, third-order ROW scheme with the time step of  $1 \times 10^{-4}$  were used in all simulations.

### C. Dynamic Grids Deformation

In this study, the algebraic grid deformation algorithm based on [59, 66] was used to reconstruct the whole computational domain. A fifth-order blending function with  $r_5(0) = 0$  and  $r_5(1) = 1$  was used for dynamic mesh deformation. It is written as

$$r_5(s) = 10s^3 - 15s^4 + 6s^5, \quad s \in [0, 1], \quad (7)$$

where  $s$  represents the normalized distance between the present grid node and the moving boundaries. The change in the position vector  $\vec{P}$  for an arbitrary grid node can then be obtained as follows:

$$\Delta \vec{P}_{present} = (1 - r_5) \Delta \vec{P}_{rigid}. \quad (8)$$

Note that when  $r_5(0) = 0$ , the grid node will move at the same speed with the moving boundary; and when  $r_5(1) = 1$ , the grid node will stay stationary.

### D. Computational Domain

This study used an array of cylinders to generate an unsteady flow environment for a pitching airfoil as shown in Fig. 1. The dimensions of the computational domain are loosely based on ongoing wind tunnel tests at the U.S. Army



**Table 1** Grid dimensions in the grid convergence study.  $N_{ele}$  stands for the total number of elements,  $N_g$  stands for the number of grid points surrounding either the “Airfoil” or “Cylinder”, and  $\Delta n$  stands for the size of the first-layer element in the wall normal direction of either the “Airfoil” or “Cylinder”.  $c$  is the airfoil chord length.

Grid Types	$N_{ele}$	Airfoil $N_g$	Airfoil $\Delta n$	Cylinder $N_g$	Cylinder $\Delta n$	$\overline{C_T}$	$RMS$
$St = 0.2$							
Baseline	109,460	204	$0.0005c$	40	$0.001c$	0.09710	0.1859
Coarse	54,240	104	$0.001c$	40	$0.001c$	0.09361	0.1610
$St = 0.3$							
Baseline	109,460	204	$0.0005c$	40	$0.001c$	0.23482	0.3478
Coarse	54,240	104	$0.001c$	40	$0.001c$	0.24934	0.3427

Research Lab (DEVCOM ARL). Figure 1(a) also shows the boundary conditions used in the numerical simulation. For these simulations a fixed inlet and a typical outlet boundary were used. For the top and bottom walls of the domain, inviscid wall boundary conditions were used to save computational cost while mimicking the wind tunnel wall effect. To allow the disturbances generated by the cylinders to evolve, the distance between the cylinder array and the NACA 0012 airfoil was set to  $7c$ , where  $c$  is the chord length of the airfoil. The array of cylinders was placed  $50c$  downstream of the inlet. The ratio of the distance between cylinders ( $L$ ) to the cylinder diameter ( $d$ ), i.e.  $\frac{L}{d}$  was 3. The freestream Mach number was fixed at 0.1 for all cases.

A grid sensitivity study has been conducted to ensure that the simulation results are reasonably grid independent. Two sets of grids were tested here at  $Re = 10,000$  and  $St = 0.2$  and  $St = 0.3$ , where  $Re$  is the Reynolds number based on the airfoil chord length, and  $St$  is the Strouhal number; see the grid size dimensions in Table 1. The baseline grid is shown in Figure 1 (b) for reference. When the baseline grid was coarsened by removing 50% of all elements, the mean thrust coefficients changed by 3.6% of average thrust and about 2% of the cycle-to-cycle fluctuations, as noted by the root mean square (RMS) for the  $St = 0.2$  case. Similarly, for  $St = 0.3$ , the difference between the average thrusts for coarse and baseline meshes is about 6%.

### III. Verification and Validation (V&V) of the CFD Solver

#### A. Characterization of Unsteadiness Environment

To evaluate the unsteadiness generated by the cylinder array, the flow field downstream of the array was first characterized without the airfoil. As illustrated in Fig. 2(a), the vortices produced by the cylinder array interacted with each other and decreased in intensity as they convected downstream. Weaker and less-coherent vortices were observed near the location where the airfoil would be placed in later studies, shown in Fig. 2(a), as compared to those near the cylinders. Note that for this study the leading edge of the airfoil was positioned at  $(x, y) = (0, 0)$ . A numerical probe, equivalent to a hot-wire probe in experiments but in a non-intrusive sense, was placed at  $(0, 0)$  with no airfoil present. In this study, a numerical probe is the point in the computational domain where the flow variable, such as velocity, is

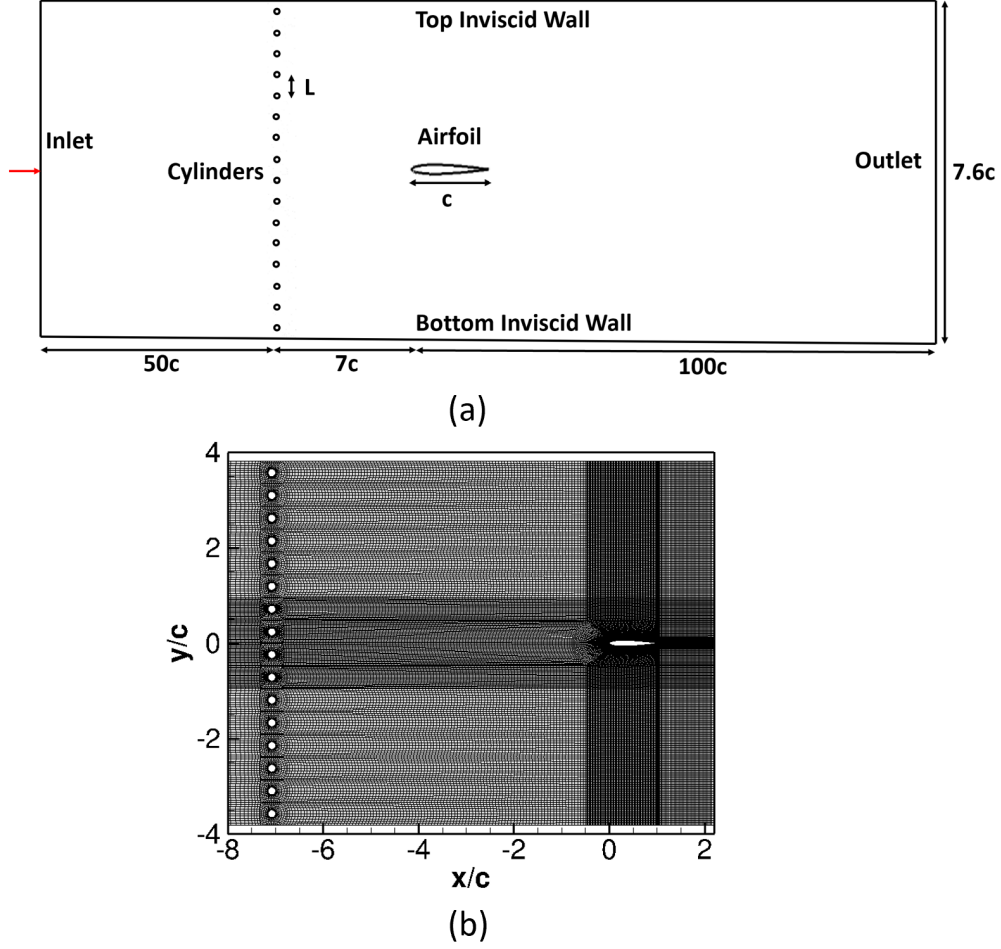


**Fig. 1** (a) Computational domain of the inline configuration of cylinders with an airfoil downstream and (b) An overview of grids around the airfoil and cylinders.

measured during simulations. Fig. 2(b) depicts the velocity power spectrum for this probe measured over 100 convective times. The power spectral density (PSD) of the velocity shows that the slope in the energy decay region is approximately  $-3$ . Rutgers [67], who placed an array of cylinders along the channel walls in a flow, observed a similar turbulence decay and energy spectrum with a  $k^{-3}$  trend on decaying 2D turbulence. Typically vortices break down into smaller scales due to 3D vortex stretching, resulting in an energy decay region of  $-\frac{5}{3}$ . This indicates that compared to 3D turbulence, 2D unsteady flow environments create larger while weaker vortex structures to interact with the oscillating airfoil. A recent study by Poudel et al. [54] evaluated the unsteadiness generated in both 2D and 3D simulations. That study showed that the overall structure of the flow was similar, with large vortical structures moving downstream from the cylinder array. The primary difference between 2D and 3D simulations is the decay and dissipation of large vortical structures. Therefore, conclusions from 2D simulations based on time- and space-averaged phenomena can be readily extended to 3D; see, for example, a work by Visbal [64] under uniform flow conditions.

Several Reynolds numbers, where Reynolds number is defined as  $Re = U_{\infty}c/\nu$  and  $c$  is the airfoil chord length, were

examined in this study. These chord based Reynolds number varied from  $Re = 500$  to  $10,000$ . This causes the Reynolds number, based on the diameter of the cylinders, to vary since the ratio of the airfoil chord length to the diameter of the cylinder is approximately 3.8. The airfoil was placed in the domain and a separate probe was placed one chord length (i.e., at  $(-1, 0)$  here) upstream of the airfoil to capture the unsteadiness with the model present. The turbulence intensity ( $TI$ ), defined as the ratio between the standard deviation of the total velocity fluctuation to the mean velocity, at the probe location for different Reynolds numbers tested is presented in Table 2. Note that the Reynolds numbers in Table 2 are based on the chord length of the airfoil. As shown in Table 2, the turbulence intensity increases as the Reynolds number increased, which was caused by the method of generating unsteadiness in this study. The results in Table 2 are in line with those from Watkins *et al.* [68], which documented that turbulence intensity can easily exceed 25% at low Reynolds numbers.

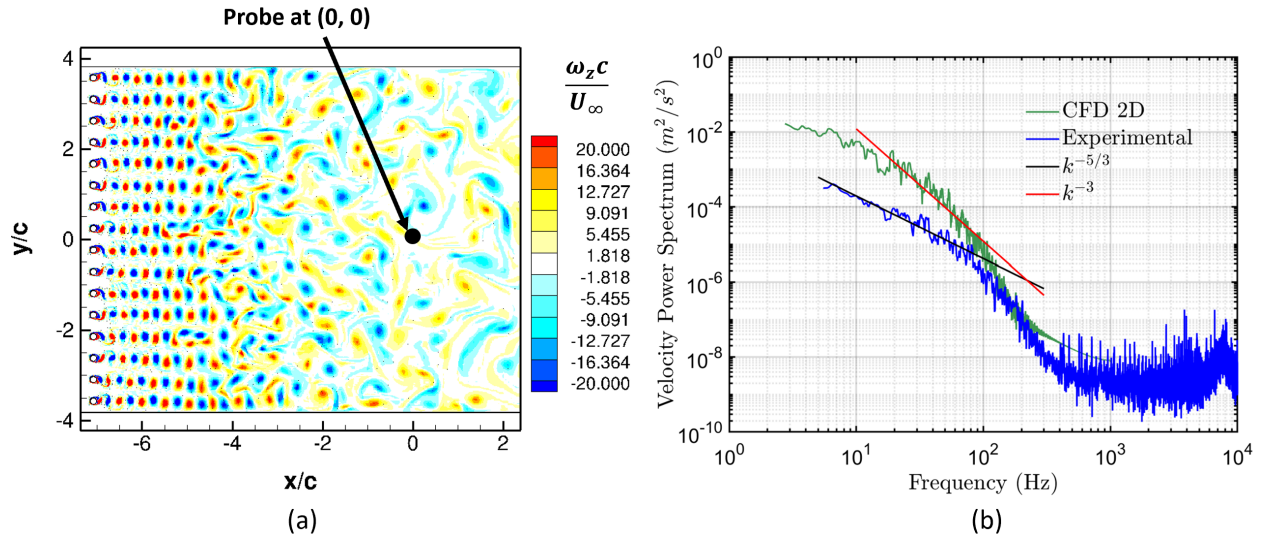


**Fig. 2** (a) 2D flow field in the downstream of an array of cylinders and (b) Velocity Power Spectrum plot at the probe location  $(0, 0)$ .

**Table 2** Turbulence Intensity for different Reynolds Numbers at probe location  $(-1, 0)$

Reynolds Numbers ( $Re$ )	Turbulence Intensity ( $TI\%$ )
500	15.83
2,000	27.65
4,000	36.68
7,000	38.43
10,000	42.09

## B. Airfoil Kinematics and Moving Grid Simulation V&V

In this study, a NACA0012 airfoil was pitched with a sinusoidal motion about its 1/4 chord axis, specifically expressed as:

$$\theta(t) = \theta_m + \theta_0 \sin(2\pi f t + \phi), \quad (9)$$

where  $\theta_m$  is the mean angle of attack,  $\theta_0$  is the amplitude of the pitching angle,  $\phi$  is the initial phase,  $f$  is the oscillating frequency, and  $t$  is the dimensional time. These types of problems are typically classified by using reduced frequency,  $k$ , and Strouhal number,  $St$ , defined as

$$k = \frac{\pi f c}{U_\infty}, \text{ and } St = \frac{2f A_{pitch}}{U_\infty}, \quad (10)$$

where  $c$  is the chord length of the airfoil,  $A_{pitch}$  is the pitching amplitude of the trailing edge of the airfoil, and  $U_\infty$  is the freestream velocity. In this work, following Senturk and Smits [10], only Strouhal number will be used to characterize flow features. Strouhal numbers ranging from 0.1 to 0.4 were tested, as shown in Table 3. Note that the pitching amplitude for all these cases was fixed at  $\theta_o = 8^\circ$ , which will result in different reduced frequencies. To allow the flow to fully develop the simulations were run for 15, 30, and 40 oscillation cycles for Strouhal numbers of 0.1, 0.2, and 0.3 respectively. When time averaged statistics are reported, the final 5, 10, and 20 cycles were averaged depending on the Strouhal number.

**Table 3 : Pitching airfoil cases with varying Strouhal numbers with a fixed pitching amplitude  $\theta_o = 8^\circ$ .**

Cases	Strouhal Numbers	Reduced Frequencies
1	0.1	1.5
2	0.2	3.0
3	0.3	4.5
4	0.4	6.0

The numerical solver used in this study is the same as that in Poudel et al. [58], and has been thoroughly verified and validated with previous data from static airfoils [7, 69–71], and those from oscillating airfoils with a wide range of Strouhal numbers and reduced frequencies [72]. As will be presented in Section IV, our simulation results of pitching airfoils also have good agreement with those by Senturk and Smits [10] under uniform upstream flow conditions. More V&V details are omitted here for brevity, and interested readers are referred to [58].

## C. Boundary Conditions

When studying oscillating airfoils, especially at high Strouhal numbers, boundary conditions must be selected with sufficient care. In this study the computational domain was originally selected to align with common wind tunnel

dimensions for experimental validation [54]. This results in an inviscid wall boundary condition about 3.8 chord length away from the pitching airfoil as shown in Fig. 1. To evaluate the effect of this boundary condition the distance from the airfoil to the inviscid walls was varied from  $3.8c$  to  $50c$ , where  $c$  is the airfoil chord length.

The thrust coefficient is defined as

$$C_T = \frac{-F_x}{\rho U_\infty^2 A/2}, \quad (11)$$

where  $F_x$  is the force in x-direction,  $\rho$  is the fluid density,  $U_\infty$  is the freestream velocity and  $A$  is the planform area. Figure 3 shows the thrust coefficient history for the pitching airfoil at  $Re = 10,000$  for  $St = 0.2 - 0.4$ . For lower Strouhal numbers (i.e., 0.2 and 0.3 in this test), the inviscid wall boundary conditions enforced on the small domain had little impact on the thrust compared to those on the large domain; see Fig. 3 (a) and (b). The smaller domain merely resulted in a slight variation in the peaks and troughs of the thrust coefficients. However, at the higher Strouhal number,  $St = 0.4$ , the force history for the small computational domain became notably aperiodic from cycle to cycle, with large over-predictions of the force compared to the larger domain; see Fig. 3 (c). A similar trend was observed in the lift coefficient with minor differences at low Strouhal number but large lift deviations at  $St = 0.4$ . Interestingly, despite this apparent instantaneous force difference, the airfoil's time-averaged thrust coefficients, calculated over the last 20 periods of both numerical simulations, were 0.3229 and 0.3391 for the small and large domains, respectively. The same phenomenon was observed at different Reynolds numbers. This demonstrates the risk of evaluating computational results without a close comparison of force coefficients with flow field results.

The source of the wall effects at higher Strouhal numbers is illustrated in Fig. 4, which depicts the instantaneous pressure coefficient field over a pitching airfoil at  $St = 0.2 - 0.4$  for  $Re = 10,000$  in both small and large computational domains. The pressure wave reflection from the inviscid wall was mild for the lower Strouhal number, as shown in Fig. 4 (a) and (c). For  $St = 0.4$  pressure waves were reflected back to the airfoil from the top and bottom walls, interacting with the airfoil (Fig. 4e). This indicates that for higher Strouhal numbers, even though the average forces from a small computational domain may be close to those from a large domain, the flow behavior can be highly affected by the inviscid walls in the computational domain. In the current study, the Strouhal number was kept below  $St = 0.3$  to minimize the near-wall effects.

## IV. Results and Discussion

### A. Uniform Flow Baseline

First the baseline behavior of a pitching airfoil with a fixed pitching amplitude  $\theta_0 = 8^\circ$  in uniform flow conditions was calculated for comparison with those in unsteady flow environments discussed later. For this baseline the Strouhal number was varied from 0.1 to 0.3 at different Reynolds numbers based on the airfoil chord length, namely, 500, 2,000,

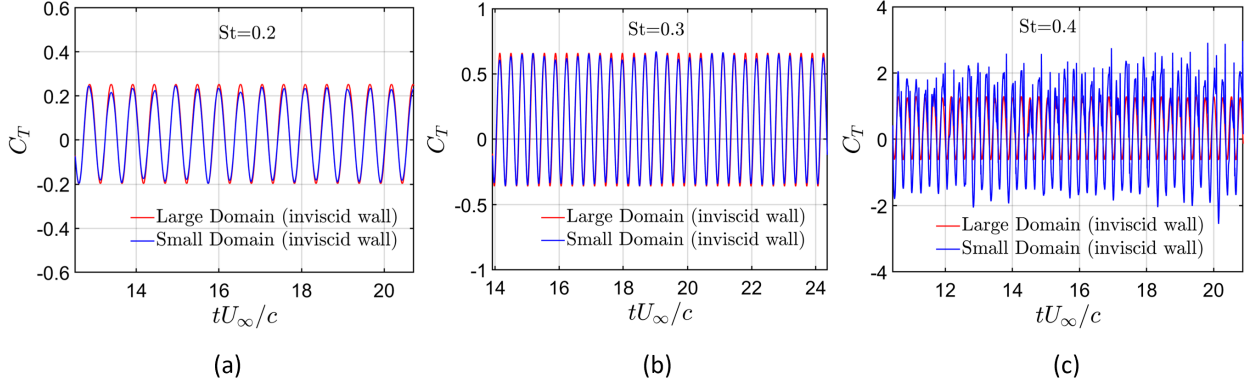


**Fig. 3 Thrust coefficient under uniform flow conditions at (a)  $St = 0.2$ , (b)  $St = 0.3$  and (c)  $St = 0.4$  for  $Re = 10,000$  for large and small computational domains.**

4,000, 7,000, 10,000, and 30,000.

These results were compared with results from Senturk and Smits [10], shown in Fig. 5 (a), in which thrust production of oscillating airfoils were numerically analyzed. Fig. 5 (a) presents the average thrust coefficients for different Reynolds numbers over a range of Strouhal numbers, and Fig. 5 (b) depicts the same information but plotted against Reynolds number for later comparisons. The results of the current study agreed well with those from Senturk and Smits [10]. A key observation is that increasing Reynolds number acts to increase mean thrust generation at a fixed Strouhal number. These results also make clear that the airfoil generates drag at low Reynolds and Strouhal numbers in uniform flow conditions. Further, the mean thrust coefficient shows asymptotic behavior with increasing Reynolds numbers. This was also observed by Senturk and Smits [10]. These results suggest that the boundary layers on the airfoil, which provide the source vorticity for thrust production, reach a maximum vorticity generation state. This is likely due to the transition of the boundary layers from laminar to turbulent. Figures 6 and 7 show the flow evolution with Reynolds number, which appears to be approaching a limit.

An analysis of the flow fields was also carried out to identify key flow features at different Reynolds and Strouhal numbers. Figures 6 and 7 show the normalized vorticity fields around the oscillating airfoils at Strouhal numbers of  $St = 0.1$  and  $0.3$ , respectively. Flow fields at  $St = 0.1$  and lower Reynolds numbers (i.e., 500 and 2,000 here) showed typical von Kármán vortex street features, a typical drag production wake type. The vorticity fields at  $St = 0.1$  and higher Reynolds numbers (i.e., 10,000 and 30,000 here) showed unsteady wake structures, which does not create net drag or thrust. At  $St = 0.3$ , reverse von Kármán vortex streets were observed at all Reynolds numbers. Although the presence of a reverse von Kármán vortex street indicates that there exists a jet in the wake of the airfoil, it does not necessarily create thrust on the airfoil at low Reynolds numbers, such as the  $Re = 500$  case presented here; see similar discussions from Bohl and Koochesfahani [73]. At larger Reynolds numbers where the inviscid flow interaction dominates, the reverse von Kármán vortex street is an indication of thrust production over the upstream airfoil; see the

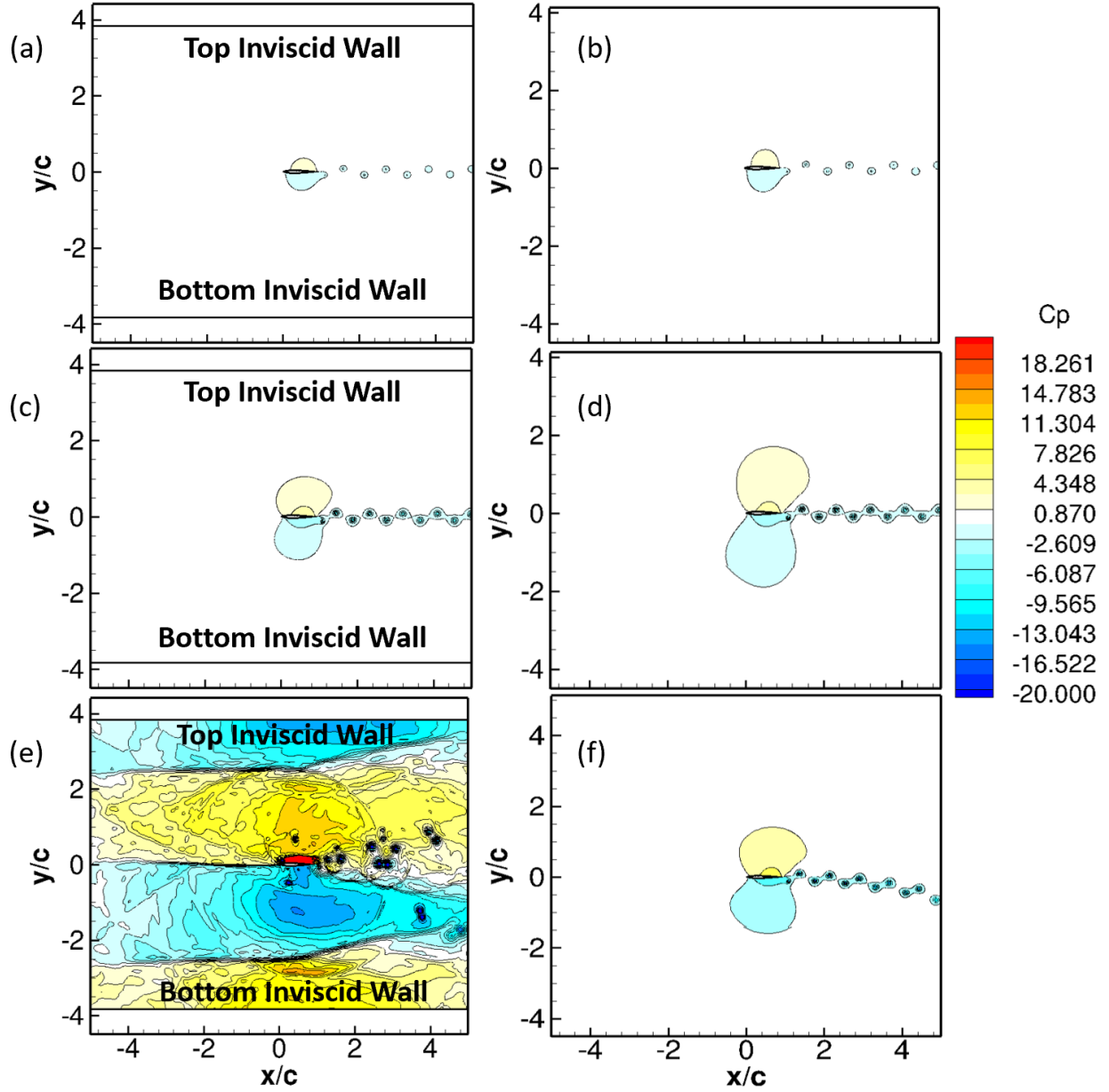


**Fig. 4** Instantaneous pressure coefficient fields at (a), (b)  $St = 0.2$ , (c), (d)  $St = 0.3$  and (e), (f)  $St = 0.4$  for  $Re = 10,000$  in small computational domains similar to that in wind tunnel tests (left) and large computational domain (right).

correspondence between Fig. 5 and Fig. 7 for the high Reynolds number cases, e.g.,  $Re = 2,000$ ,  $10,000$  and  $30,000$ .

### B. Pitching Airfoils in Non-uniform Upstream Flows

This section investigates the effect of non-uniform flow environments created by an upstream array of cylinders on the propulsive performance of a pitching airfoil. Flow fields are presented to better understand how non-uniform incoming flows alter the underlying physics related to the interaction. The Reynolds numbers based on the airfoil chord

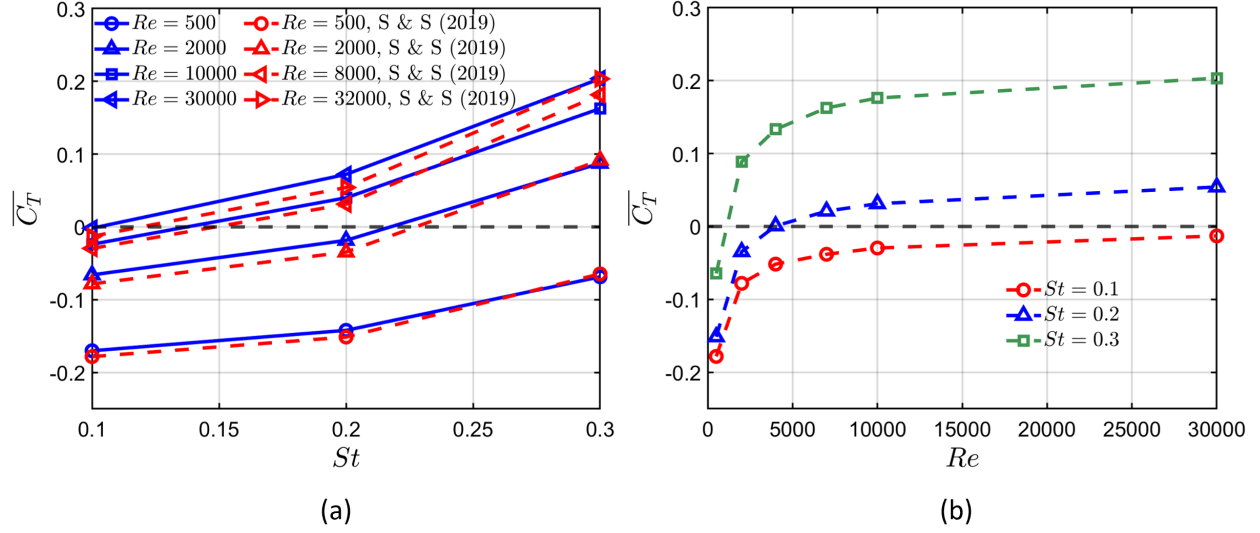


**Fig. 5** (a) Time-averaged thrust coefficients over the pitching airfoil under uniform flow conditions (a) as a function of  $St$  for different Reynolds numbers and comparison with Sentruk & Smits [10] and (b) as a function of  $Re$  for different Strouhal numbers.

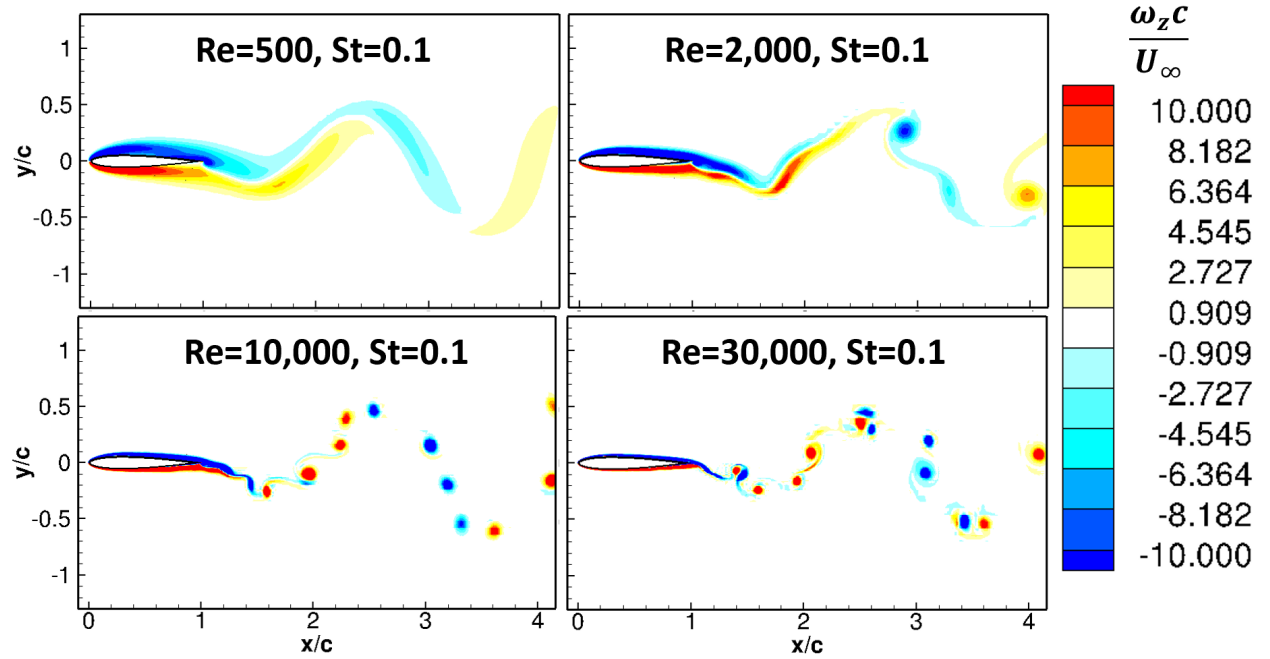


**Fig. 6** Instantaneous vorticity fields over a pitching airfoil under uniform flow conditions at  $St = 0.1$ .

length were varied from 500 to 10,000 in this section, while all other variables were kept the same as those under uniform flow conditions.



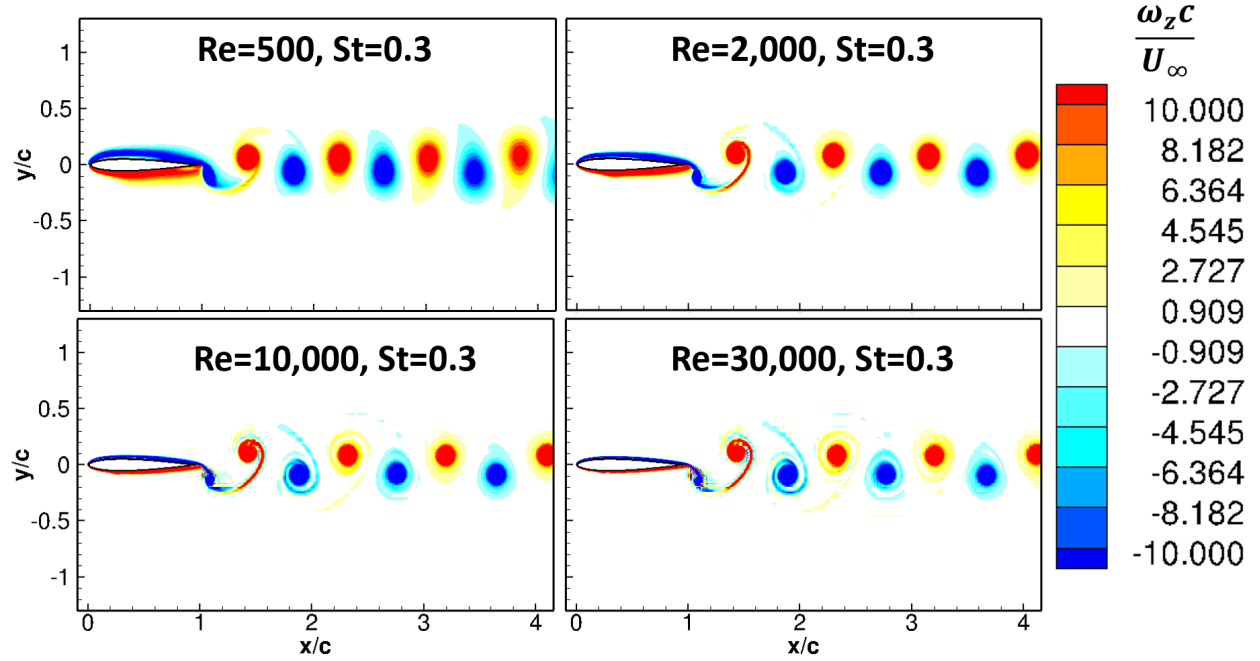


**Fig. 7** Instantaneous vorticity fields over a pitching airfoil under uniform flow conditions at  $St = 0.3$ .

### 1. Visualization of instantaneous flow fields and aerodynamic forces

Figure 8 shows the time histories of thrust coefficients at different Strouhal numbers for different Reynolds numbers. Therein, the periodic time histories of thrust coefficients at  $St = 0.1$  and two Reynolds numbers, i.e.,  $Re = 500$  and  $Re = 10,000$ , in uniform upstream flows were also presented for comparison purposes. In general the thrust coefficients show irregular fluctuations due to unsteadiness in the ambient flow environment. At  $St = 0.1$ , except for  $Re = 500$ , the thrust coefficient histories at different Reynolds numbers have more intense fluctuations compared to those at higher Strouhal numbers. Similar to the observations from [58] where the interaction between gusts and an oscillating airfoil is investigated, energetic pitching motions can suppress the unsteady effect from ambient flows. Moreover, as will be presented in the next subsection, the pitching motion can also take advantage of the energy-containing unsteady ambient flows to boost thrust production.

Fig. 9 depicts the instantaneous vorticity fields for Reynolds number 500 at  $St = 0.2$  and  $St = 0.3$  under non-uniform flow conditions. The vortices in the ambient flow were observed to have a limited effect on the airfoil's boundary layer due to their lower strength, when compared with the vortices created by the pitching airfoil. The reverse von Kármán vortex street was slightly deflected by the ambient flow unsteadiness (see Fig. 9(b)), when compared to the horizontal wake shown in Fig. 7. This was especially true at higher Strouhal numbers and is similar to the observations from the interaction between an oscillating airfoil and a weak shear layer as reported in [74, 75]. It should be noted that the interaction between the wakes and the incoming unsteady vortical flow results in weak cycle-to-cycle changes in the wake structures, which are not stable. One potential cause of the wake deflections observed here, which typically only

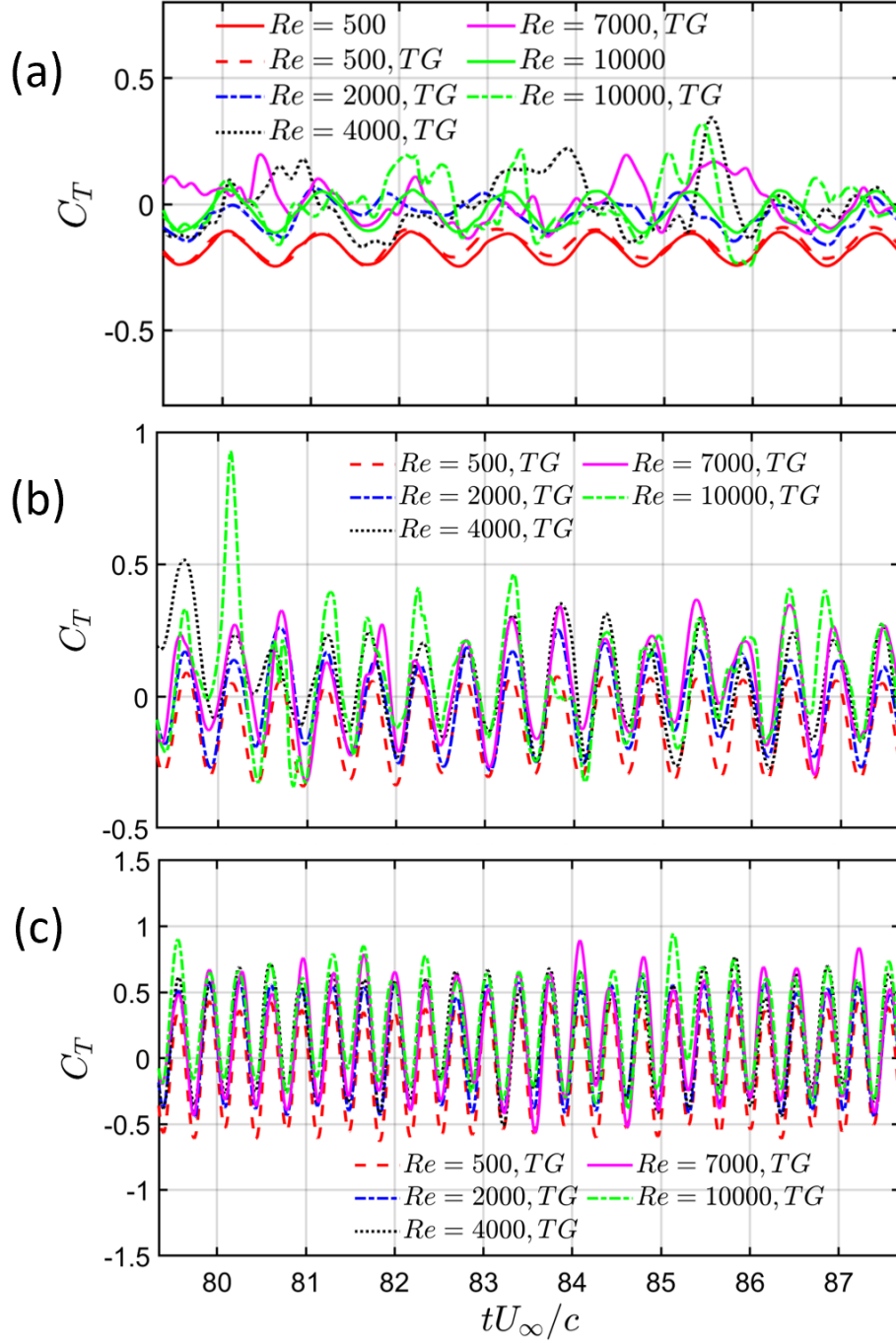


**Fig. 8** Instantaneous thrust coefficient histories for the pitching airfoil under non-uniform flow conditions at different (a)  $St = 0.1$ , (b)  $St = 0.2$  and (c)  $St = 0.3$  for different  $Re$ .

appear when the reverse von Karman wake is present, may be due to the downstream vortical structures present in the unsteady flow. It is possible that the wake deflection behavior may be related to the downstream flow conditions and not necessarily the reverse von Karman wake itself, but further study would be needed for a full understanding.

The two dimensional nature of the current study must also be assessed at this stage. In the cases studied here the

flow is dominated by the oscillating frequency and shed vortices, as shown in the oscillatory nature of thrust coefficient in Fig. 8. It has been shown by Visbal [64] that 2D and 3D simulations of a plunging airfoil agreed well using an ILES approach at a Reynolds number of 40,000. In a different study by Golubev et al. [76], the aerodynamic responses to impinging vortical structures on the suction side of an airfoil at  $Re=60,000$  revealed a very close comparison for lift time histories from 2D and 3D ILES simulations. Based on the 2D and 3D simulations, the peak values for both responses appeared to be very close. It should be noted that only one vortex interacts with the airfoil in this study. While a 3D simulation would result in faster dissipation of the incoming unsteadiness, adjustments could reasonably be made to match the levels of unsteadiness used in the current study. Results presented later will show that the effects of unsteadiness would be unlikely to change in environments with higher dissipation, since the source of those changes would be somewhat unaffected by dissipation if the level of unsteadiness were comparable.

The wakes become more chaotic as the Reynolds numbers increase due to the intense interactions between the upstream vortices and oscillating airfoil wakes; see Fig. 10 (a) and (b). This unsteady interaction is the driving factor behind the intense thrust fluctuations observed in Fig. 8, especially at small Strouhal numbers. One notable feature here is the large increase in magnitude of thrust and drag in some cycles. One unusual thrust boost was observed at non-dimensional time ( $t^* = tU_\infty/c$ ) around  $t^* \approx 80.15$  for the  $St = 0.2$  and  $Re = 10,000$  case, and an unusual drag increase occurred at  $t^* \approx 86$  for the  $St = 0.1$  and  $Re = 10,000$  case.

The instantaneous vorticity and pressure fields for the excess thrust case noted above are shown in Fig. 10. Just prior to the increased thrust generation, a pair of clockwise and counterclockwise vortices labeled 'A' (see Fig. 10 (a)) from the upstream unsteady flow environment are close to the leading edge of the airfoil's lower surface. At the same time, the leading edge of the airfoil is pitching up and creating the leading edge vortex (LEV) '1' on the lower surface of the airfoil. Fig. 10 (c) shows the negative pressure regions generated at this time for the vortices. As the airfoil continued pitching upward it started to interact with impinging vortex 'B', as shown in Fig. 10 (b). The combined effects of these vortices acted to create a low pressure region over the entire lower surface of the airfoil, thus producing a higher-than-usual thrust force as a favorable condition for thrust enhancement.

A different vortex interaction occurred which generated the significant drop in thrust coefficient at  $St = 0.1$  for  $Re = 10,000$  around  $t^* = 86$  in Fig. 8 (a). The flow fields around that time are shown in Fig. 11 with instantaneous vorticity and pressure fields. In this case a pair of vortices 'A' and another pair of vortices 'B' were located near the upper and lower surfaces of the airfoil, respectively, as shown in Fig. 11 (a). At this instance, the leading edge of the airfoil was pitching down, which for a fast pitch-down maneuver in a uniform incoming flow would be expected to create a high pressure region near the leading edge on the bottom surface of the airfoil, and a low pressure region on the top surface, due to the induced angle of attack. Note that this is opposite the steady aerodynamic behavior and is caused by the relative motion of the wing compared to the incoming flow. However, due to the unfavorable vortex-airfoil interaction the vortex pair 'A' suppressed the creation of a LEV, which is typically created on the top surface of the

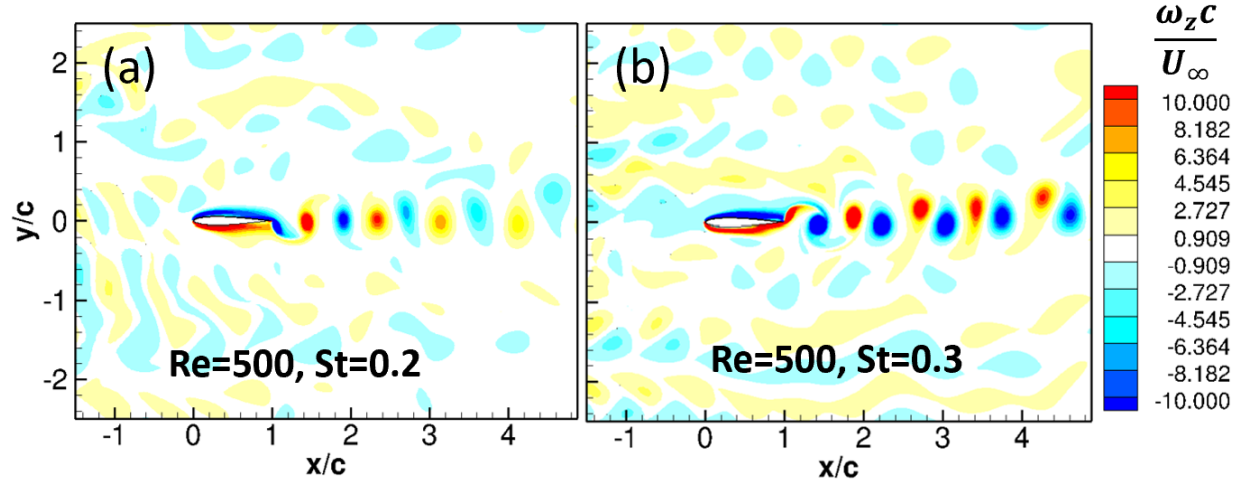


Fig. 9 Instantaneous vorticity field over the pitching airfoil under non-uniform flow conditions at  $t^* = 86.6$  (a)  $St = 0.2$  and (b)  $St = 0.3$  at  $Re = 500$ .

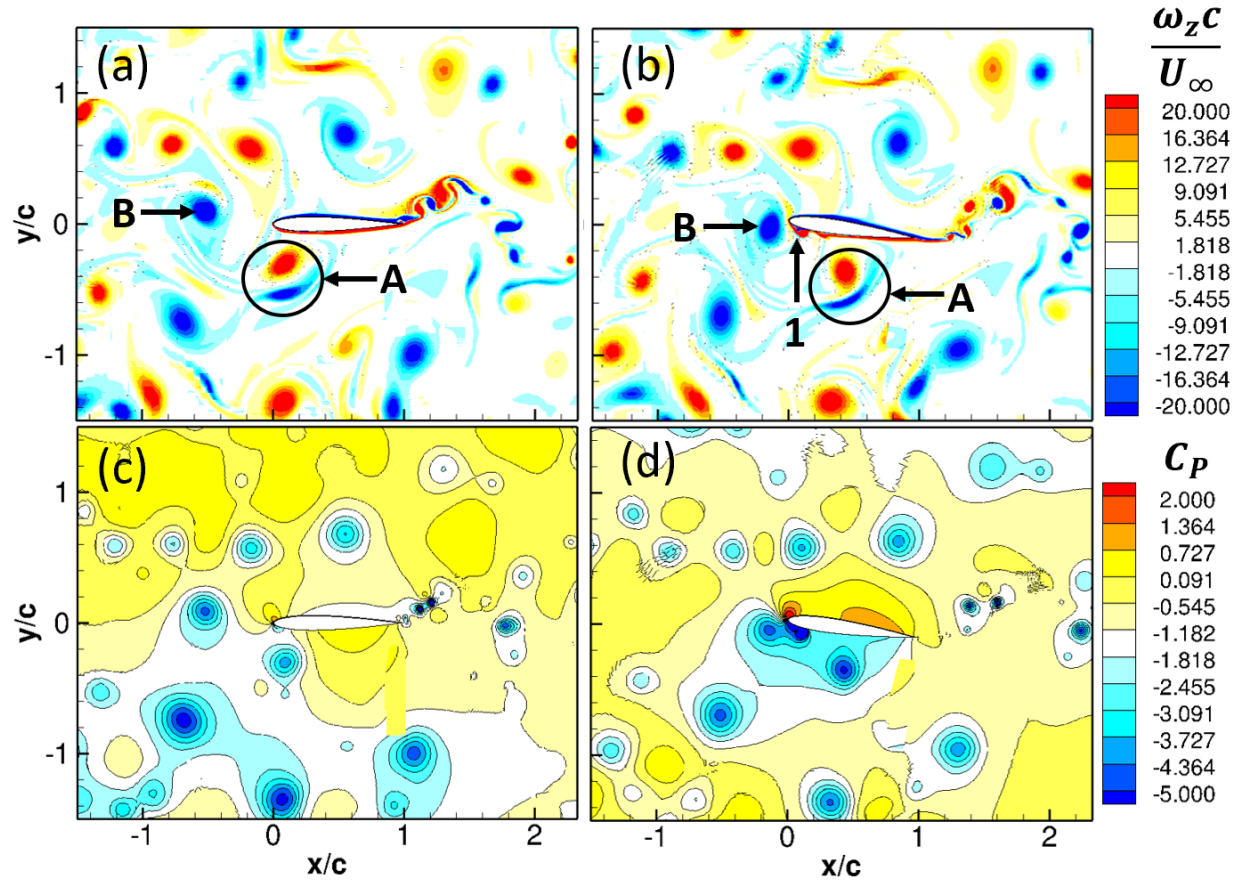
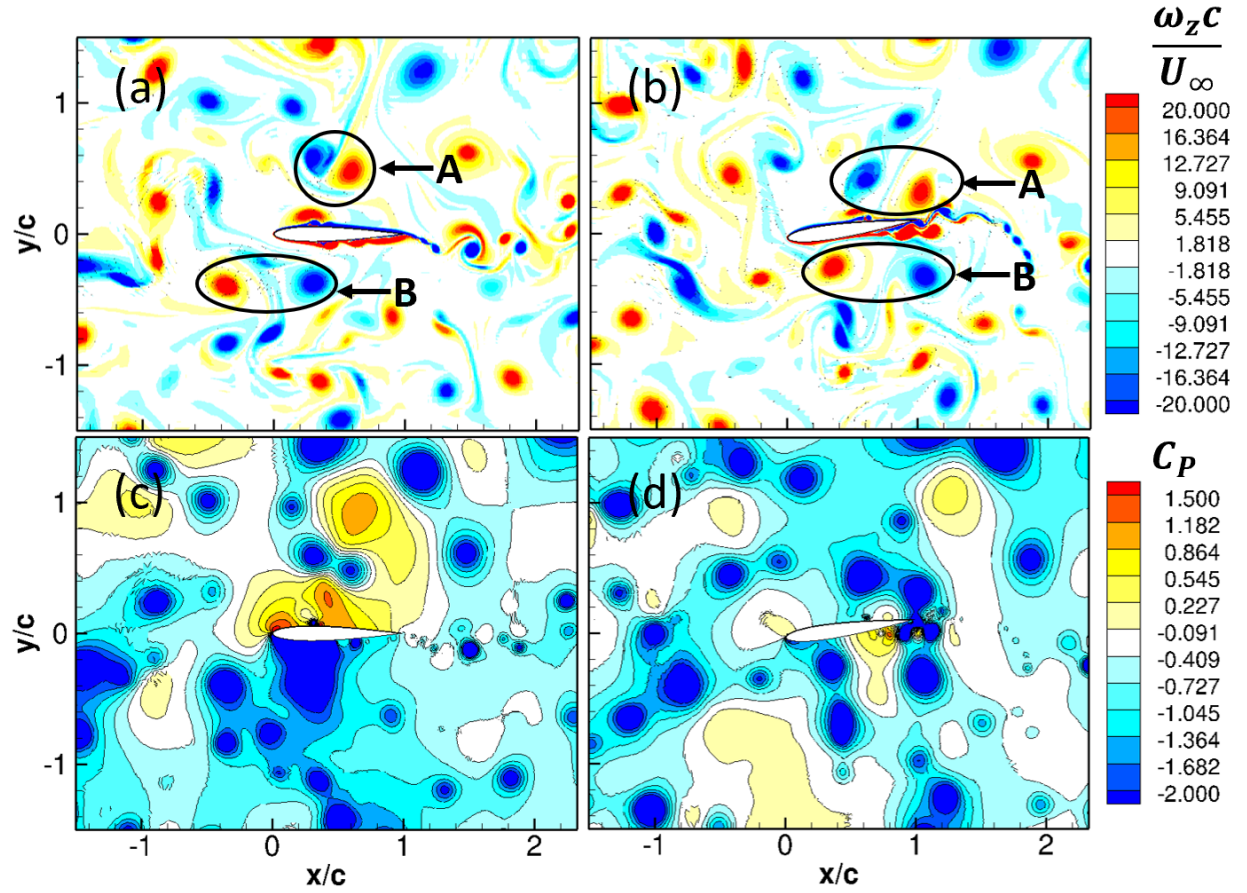


Fig. 10 Instantaneous vorticity and pressure fields over the pitching airfoil (a), (c) at  $t^* = 79.84$  and (b), (d) at  $t^* = 80.1$ , under non-uniform flow conditions at  $St = 0.2$  and  $Re = 10,000$ .

airfoil. Meanwhile, the positive vortex in 'B' induced a low pressure region on the bottom surface of the airfoil (see the pressure evolution process in Fig. 11 (c) and (d)). This type of surface pressure distribution can induce large drag over the airfoil. Further, as observed from Fig. 11 (d), the positive vortex in 'A' and the negative one in 'B' both interact with the trailing edge vortex shed from the pitching airfoil, inducing a strong low pressure region near the airfoil's trailing edge, especially over the lower surface further contributing to the drag peak.



**Fig. 11** Instantaneous vorticity and pressure fields over the pitching airfoil (a), (c) at  $t^* = 85.6$  and (b), (d) at  $t^* = 86.1$  under non-uniform flow conditions at  $St = 0.1$  and  $Re = 10,000$ .

## 2. Aerodynamic force statistics analysis

This section examines the thrust and lift statistics for the pitching airfoil in unsteady flow environments compared to those in uniform upstream flows. Fig. 12 depicts the time-averaged thrust coefficients for the oscillating airfoil at various Strouhal numbers for nominal and effective Reynolds numbers, as well as their comparison with those under uniform flow conditions. The definition of the effective Reynolds number will be introduced in this section when discussing the flow unsteadiness effects. From Fig. 12, the average thrust coefficients for unsteady upstream flow cases were found to be consistently greater than those for uniform upstream flow cases, except for the case with  $St = 0.3$  at  $Re = 500$ . As

mentioned in the previous subsection, the background vorticity at  $Re = 500$  functions more like a weak shear layer than discrete vortex structures. It has been shown by Yu et al. [74] and Hammer et al. [75] that the impact of a shear layer on thrust production of an oscillating airfoil is trivial, and can either slightly enhance or reduce thrust. The observation at  $Re = 500$  here agrees with that observation.

The time-averaged thrust coefficient is a function of the Reynolds and Strouhal numbers, i.e.,  $\overline{C_T} = f(Re, St)$ . As shown in Fig. 12 (a), the time-averaged thrust coefficients for a fixed  $St$  appear to follow the same trend as those under uniform flow conditions but cases with unsteady incoming flow consistently produced greater thrust. This suggests that the unsteadiness caused by the upstream array of cylinders has a similar effect as increasing the velocity (or Reynolds number) experienced by the airfoil.

An analysis was performed to approximate an effective Reynolds number in order to demonstrate how Reynolds number is changed due to unsteadiness. From the baseline steady data, Fig. 12(a), a polynomial relationship between  $Re$  and  $C_T$  was developed. An iterative method, based on the polynomial developed on the baseline cases, was then used to estimate the effective Reynolds number of the unsteady flow cases, the results of which are shown in Fig. 12 (b). This process had little effect when converting lower Reynolds number cases, but significantly changed higher Reynolds number unsteady flow cases. For example, the effective Reynolds number shift for the unsteady flow case with a Reynolds number of 500 was small. However, for the unsteady flow case with a Reynolds number of 7,000 the effective Reynolds number exceeds 30,000.

The correlation between the time-averaged thrust coefficient and the effective Reynolds number suggests that the effective velocity,  $U_e$  which is a nonlinear function of the nominal Reynolds number and Strouhal number, is larger than  $U_\infty$ . This indicates that the extra kinetic energy in non-uniform flows can enhance thrust production. The time-averaged lift coefficient was observed to be somewhat random due to flow unsteadiness, but was approximately zero at all Reynolds numbers.

### 3. Scaling laws:

Senturk and Smits [10] derived a simple scaling law for a pitching airfoil following the work of Floryan *et al.* [77] under uniform flow conditions. The equation for the thrust coefficient derived by these studies is:

$$\overline{C_T} = \beta St^2 - C_D, \quad (12)$$

where  $\beta$  is an empirically derived coefficient,  $St$  is Strouhal number, and  $C_D$  is the offset drag term introduced previously by Floryan *et al.* [77]. In Floryan *et al.* [77],  $C_D$  and  $\beta$  were calculated by curve fitting the data at each Reynolds number, but it should be noted that Reynolds number effects were not considered in that study. This offset drag term was considered as the equivalent fixed body drag of the pitching airfoil's projected frontal area. Later, Senturk and

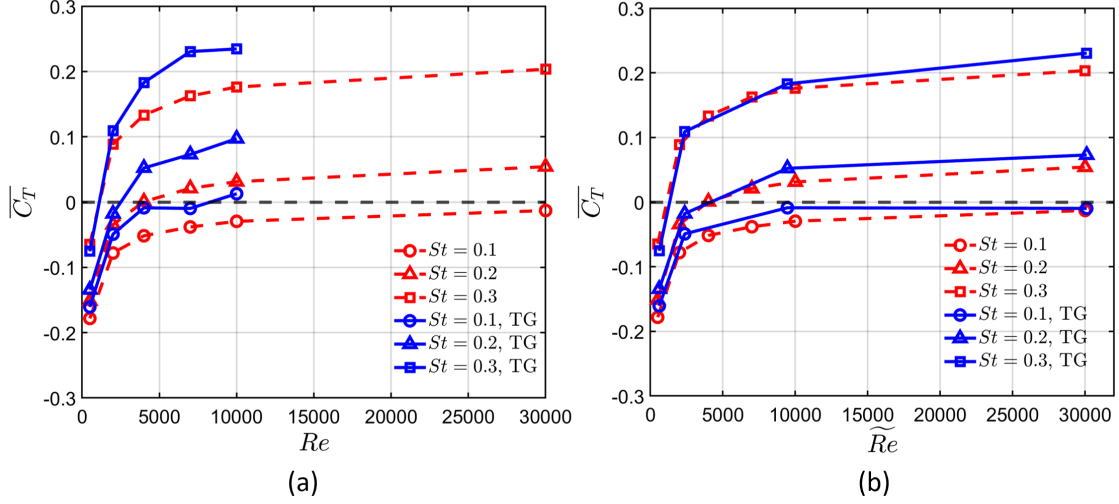


**Fig. 12** Time-averaged thrust coefficients over the pitching airfoil under non-uniform flow conditions at different  $St$  for different Reynolds numbers and comparison with those under uniform flow conditions as (a) a function of  $Re$  and (b) a function of effective  $Re$ .

Smits [10] validated the proposed definition of offset drag further by comparing the drag of a fixed NACA0012 airfoil at zero angle of attack to the offset drag of a pitching airfoil with  $\theta_o = 8^\circ$ . They determined that both the static drag and the offset drag of the NACA0012 airfoil decrease with increasing Reynolds number. However, the static drag of NACA0012 is significantly less than the offset drag at any Reynolds number. The values of  $C_D$  and  $\beta$  were calculated at each Reynolds number and Strouhal number combination for the uniform flow cases, using the same method as Senturk and Smits [10], and plotted in Fig. 13. Figure 13 (a) shows that the time averaged thrust coefficients align linearly to the scaling parameters, further validating the work of Senturk and Smits [10]. Figure 13 (b) shows that the offset drag and  $\beta$  change as the Reynolds number increases. The dashed lines in Fig. 13 (b) were plotted using the equations for  $C_D$  (black dashed line) and  $\beta$  (blue dashed line) from Senturk and Smits [10]. Overall, the baseline uniform flow results aligned well with prior studies.

Extending this scaling law directly to the unsteady flow cases results in an expected increase in the thrust coefficient. Figure 14(a) shows the unsteady flow thrust coefficients in blue, with the blue dashed line representing the best-fit version of the scaling law developed by Senturk and Smits [10], which is plotted as a black dashed line. A clear shift between the scaling laws is present with the most obvious being a shift in  $\Delta C_D$ . However, it should be noted that when  $\beta$  and  $C_D$  are evaluated using the effective Reynolds number, introduced in previous subsections, the thrust coefficient satisfies the original scaling law Eq. 12. However, the effective Reynolds number developed here cannot be used to predict thrust as it was calculated from the measured thrust coefficient (see Section IV.B.2). Thus, for predictive purposes, the scaling law should be built from easy-to-measure non-dimensional quantities, such as the Strouhal and Reynolds numbers in its original version.

To align the new unsteady flow data with the steady flow scaling law the offset drag  $C_D$  needs to be decreased. To



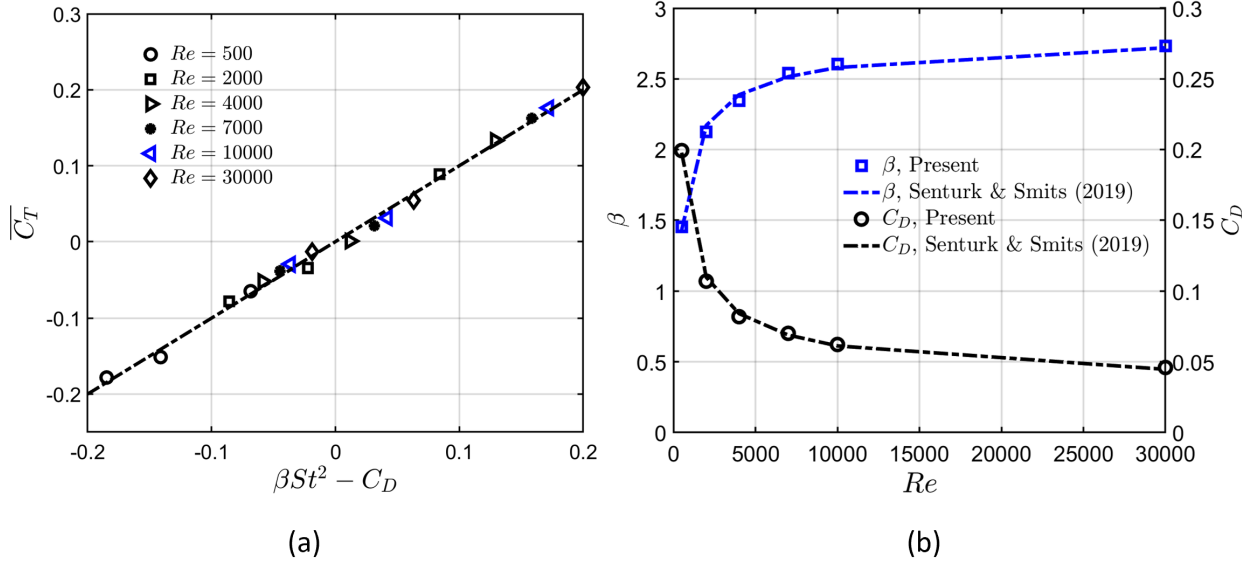


**Fig. 13** (a) Comparison with the scaling law at different  $St$  for different Reynolds numbers and (b)  $\beta$  and  $C_D$  as a function of  $Re$  under uniform flow conditions.

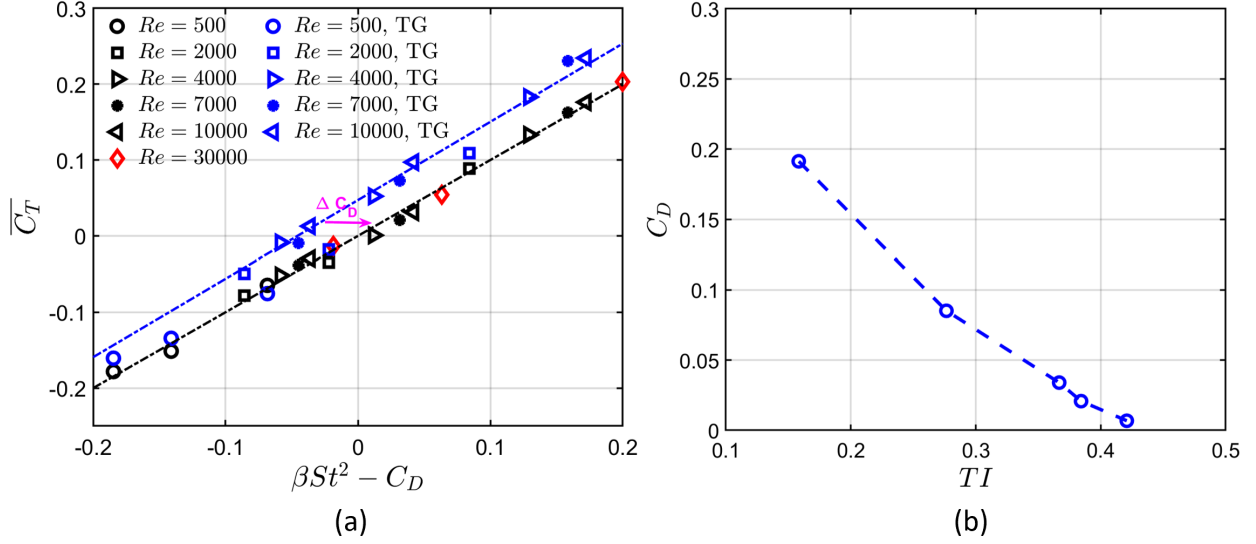
accomplish this corrected  $C_D$  values at each Reynolds number were determined for unsteady flow conditions while holding  $\beta$  constant. Since Fig. 13 showed that  $C_D$  is a function of Reynolds number it therefore becomes logical to include the turbulence intensity ( $TI$ ) in the new definition of  $C_D$  for non-uniform flow conditions. Figure 14(b) shows that  $C_D$  is also an approximately linear function of the turbulence intensity, which can be updated from the definition in Senturk and Smits [10] as the new equation for the offset drag:

$$C_D = -0.2725 TI + 3.3198 Re^{-0.5} + 0.0856 \quad (13)$$

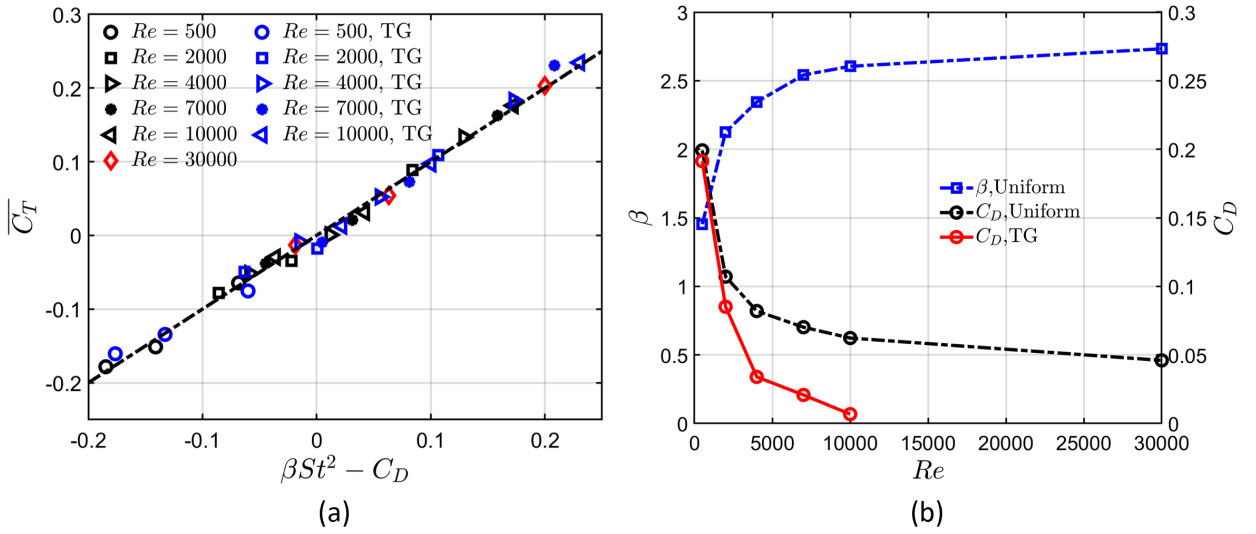
It should be noted that due to the method of unsteadiness generation used in the current study,  $TI$  was also a function of Reynolds number (see Table 2). However, Table 2 shows that  $TI$  did not increase linearly with Reynolds number. Since the data from Senturk and Smits [10] also showed a  $Re^{-0.5}$  relationship, the linear relationship between observed  $C_D$  and  $TI$  in Eq. 13 suggests the method of generating  $TI$  has little impact on the  $Re^{-0.5}$  relationship shown in Eq. 13.

Figure 15(a) shows the implementation of Eq. 13 into the scaling law with both steady and unsteady flow conditions plotted. When applying the new formulation of  $C_D$  the data correlate well with data for uniform flow conditions and align well with the original model of Senturk and Smits [10]. Figure 15 (b) shows the different  $\beta$  and  $C_D$  values as a function with Reynolds numbers. Note here that the offset drag terms vary significantly between the unsteady and baseline conditions. For uniform flow conditions the values of  $C_D$  closely aligned with Senturk and Smits' results [10]. However, for non-uniform flow conditions, the  $C_D$  followed a similar trend but with smaller values compared to the baseline flow. This trend is similar to the shift in Reynolds number observed previously in this study, which suggests that unsteadiness and Reynolds number have similar effects on the flow.





**Fig. 14** (a) Comparison of the scaling law under non-uniform flow conditions at different  $St$  for different Reynolds numbers with that under uniform flow conditions, and (b)  $C_D$  as the function of Turbulence Intensity.



**Fig. 15** (a) Comparison of the scaling law under non-uniform flow conditions at different  $St$  for different Reynolds numbers with corrected  $C_D$  with that under uniform flow conditions, and (b)  $\beta$  and  $C_D$  as a function of  $Re$  under uniform and non-uniform flow conditions.

## V. Conclusion

The present work documents the influence of unsteady flow environments on a pitching airfoil using an in-house high-order CFD solver. The unsteady flow environments were created by placing cylinders upstream of the oscillating airfoil. Steady and unsteady incoming flow conditions were compared and flow physics of thrust enhancement mechanisms of unsteady environments was explored. The unsteady flow environment served to alter oscillating wing performance in two key ways: altering the effective Reynolds number and shifting the value of the offset drag.

The unsteadiness in the flow caused an increase in thrust generation at lower Reynolds numbers, which caused low Reynolds number oscillating airfoils in unsteady flow to behavior similar to higher Reynolds number cases in steady environments. A simple fit-based correction method showed that an effective Reynolds number can be used to model the shift caused by the unsteady freestream.

The underlying flow physics showed that unsteadiness in the freestream expectedly generated variations in the sinusoidal thrust data. This unsteadiness was directly related to the large, coherent incoming flow structures. The increase in average thrust coefficient was shown to be caused by constructive interaction of freestream vortex structures and the oscillating airfoil. Drag inducing interactions were also observed but were less common than thrust increasing events, resulting in a higher average thrust. It should be noted that the scope of the current study has been limited to two dimensions and thus true turbulence was not fully modeled here. However, the interaction of coherent flow structures with the oscillating wing is a flow feature not likely to be significantly altered by the increased dissipation rates of three dimensional studies.

An extension to the thrust model proposed by Senturk and Smits [10] was developed to incorporate the effects of unsteady flow environments. An increase in thrust production was incorporated into the offset drag term of the scaling law. A linear relationship between the turbulence intensity and offset drag was demonstrated to accurately recover thrust produced in unsteady flow environments back onto the original scaling law built for uniform flow conditions.

## Acknowledgments

Research was sponsored by the Army Research Laboratory and was accomplished under Cooperative Agreement Number W911NF-20-2-0028. The views and conclusions contained in this document are those of the authors and should not be interpreted as representing the official policies, either expressed or implied, of the Army Research Laboratory or the U.S. Government. The U.S. Government is authorized to reproduce and distribute reprints for Government purposes notwithstanding any copyright notation herein. The hardware used in the computational studies is part of the UMBC High Performance Computing Facility (HPCF). The facility is supported by the U.S. National Science Foundation through the MRI program (grant nos. CNS-0821258, CNS1228778, and OAC-1726023) and the SCREMS program (grant no. DMS-0821311), with additional substantial support from the University of Maryland, Baltimore County (UMBC).

## References

- [1] Liu, H., Kolomenskiy, D., Nakata, T., and Li, G., “Unsteady bio-fluid dynamics in flying and swimming,” *Acta Mechanica Sinica*, Vol. 33, No. 4, 2017, pp. 663–684. <https://doi.org/10.1007/s10409-017-0677-4>.
- [2] SureshBabu, A., Medina, A., Rockwood, M., Bryant, M., and Gopalarathnam, A., “Theoretical and experimental investigation

- of an unsteady airfoil in the presence of external flow disturbances,” *Journal of Fluid Mechanics*, Vol. 921, 2021. <https://doi.org/10.1017/jfm.2021.484>.
- [3] Lissaman, P. B., and Shollenberger, C. A., “Formation flight of birds,” *Science*, Vol. 168, No. 3934, 1970, pp. 1003–1005. <https://doi.org/10.1126/science.168.3934.1003>.
  - [4] Liao, J. C., Beal, D. N., Lauder, G. V., and Triantafyllou, M. S., “Fish exploiting vortices decrease muscle activity,” *Science*, Vol. 302, No. 5650, 2003, pp. 1566–1569. <https://doi.org/10.1126/science.1088295>.
  - [5] Wu, X., Zhang, X., Tian, X., Li, X., and Lu, W., “A review on fluid dynamics of flapping foils,” *Ocean Engineering*, Vol. 195, 2020, p. 106712. <https://doi.org/10.1016/j.oceaneng.2019.106712>.
  - [6] Garrick, I. E., “Propulsion of a Flapping and Oscillating Airfoil,” Tech. Rep. 537, National Advisory Committee for Aeronautics Langley Memorial Aeronautical Lab, 1936.
  - [7] Liu, H., and Kawachi, K., “A Numerical Study of Undulatory Swimming,” *Journal of Computational Physics*, Vol. 155, No. 2, 1999, pp. 223–247. <https://doi.org/10.1006/jcph.1999.6341>.
  - [8] Ramamurti, R., and Sandberg, W., “Simulation of Flow about Flapping Airfoils using Finite Element Incompressible Flow Solver,” *AIAA Journal*, Vol. 39, No. 2, 2001, pp. 253–260. <https://doi.org/10.2514/2.1320>.
  - [9] Mackowski, A. W., and Williamson, C. H. K., “Direct measurement of thrust and efficiency of an airfoil undergoing pure pitching,” *Journal of Fluid Mechanics*, Vol. 765, 2015, pp. 524–543. <https://doi.org/10.1017/jfm.2014.748>.
  - [10] Senturk, U., and Smits, A. J., “Reynolds Number Scaling of the Propulsive Performance of a Pitching Airfoil,” *AIAA Journal*, Vol. 57, No. 7, 2019, pp. 2663–2669. <https://doi.org/10.2514/1.J058371>.
  - [11] Badrya, C., Govindarajan, B., Medina, A., Joon Yang, S., and Chopra, I., “Unsteady Aerodynamic Characteristics of Pitching Flat Plates at Low Reynolds Numbers,” *Journal of Aircraft*, Vol. 58, No. 4, 2021, pp. 917–934. <https://doi.org/10.2514/1.C036028>.
  - [12] Catlett, M. R., Anderson, J. M., Badrya, C., and Baeder, J. D., “Unsteady response of airfoils due to small-scale pitching motion with considerations for foil thickness and wake motion,” *Journal of Fluids and Structures*, Vol. 94, 2020, p. 102889. <https://doi.org/10.1016/j.jfluidstructs.2020.102889>.
  - [13] Mohamed, A., Massey, K., Watkins, S., and Clothier, R., “The attitude control of fixed-wing MAVS in turbulent environments,” *Progress in Aerospace Sciences*, Vol. 66, 2014, pp. 37–48. <https://doi.org/10.1016/j.paerosci.2013.12.003>.
  - [14] Watkins, S., Thompson, M., Loxton, B., and Abdulrahim, M., “On low altitude flight through the atmospheric boundary layer,” *International Journal of Micro Air Vehicles*, Vol. 2, No. 2, 2010, pp. 55–68. <https://doi.org/10.1260/1756-8293.2.2.55>.
  - [15] Watkins, S., Burry, J., Mohamed, A., Marino, M., Prudden, S., Fisher, A., Kloet, N., Jakobi, T., and Clothier, R., “Ten questions concerning the use of drones in urban environments,” *Building and Environment*, Vol. 167, 2020, p. 106458. <https://doi.org/10.1016/j.buildenv.2019.106458>.

- [16] Muhawenimana, V., Wilson, C., Ouro, P., and Cable, J., “Spanwise Cylinder wake hydrodynamics and fish behavior,” *Water Resources Research*, Vol. 55, No. 11, 2019, pp. 8569–8582. <https://doi.org/10.1029/2018WR024217>.
- [17] Ravi, S., Crall, J. D., McNeilly, L., Gagliardi, S. F., Biewener, A. A., and Combes, S. A., “Hummingbird flight stability and control in freestream turbulent winds,” *Journal of Experimental Biology*, Vol. 218, No. 9, 2015, pp. 1444–1452. <https://doi.org/10.1242/jeb.114553>.
- [18] Ravi, S., Kolomenskiy, D., Engels, T., Schneider, K., Wang, C., Sesterhenn, J., and Liu, H., “Bumblebees minimize control challenges by combining active and passive modes in unsteady winds,” *Scientific reports*, Vol. 6, No. 1, 2016, pp. 1–10. <https://doi.org/10.1038/srep35043>.
- [19] Engels, T., Kolomenskiy, D., Schneider, K., Lehmann, F.-O., and Sesterhenn, J., “Bumblebee flight in heavy turbulence,” *Physical review letters*, Vol. 116, No. 2, 2016, p. 028103. <https://doi.org/10.1103/PhysRevLett.116.028103>.
- [20] Crall, J., Chang, J., Oppenheimer, R., and Combes, S., “Foraging in an unsteady world: bumblebee flight performance in field-realistic turbulence,” *Interface Focus*, Vol. 7, No. 1, 2017, p. 20160086. <https://doi.org/10.1098/rsfs.2016.0086>.
- [21] Jakobi, T., Kolomenskiy, D., Ikeda, T., Watkins, S., Fisher, A., Liu, H., and Ravi, S., “Bees with attitude: the effects of directed gusts on flight trajectories,” *Biology open*, Vol. 7, No. 10, 2018. <https://doi.org/10.1242/bio.034074>.
- [22] Ortega-Jimenez, V. M., Greeter, J. S., Mittal, R., and Hedrick, T. L., “Hawkmoth flight stability in turbulent vortex streets,” *Journal of Experimental Biology*, Vol. 216, No. 24, 2013, pp. 4567–4579. <https://doi.org/10.1242/jeb.089672>.
- [23] Ortega-Jimenez, V. M., Sapir, N., Wolf, M., Variano, E. A., and Dudley, R., “Into turbulent air: size-dependent effects of von Kármán vortex streets on hummingbird flight kinematics and energetics,” *Proceedings of the Royal Society B: Biological Sciences*, Vol. 281, No. 1783, 2014, p. 20140180. <https://doi.org/10.1098/rspb.2014.0180>.
- [24] Ortega-Jimenez, V. M., Badger, M., Wang, H., and Dudley, R., “Into rude air: hummingbird flight performance in variable aerial environments,” *Philosophical Transactions of the Royal Society B: Biological Sciences*, Vol. 371, No. 1704, 2016, p. 20150387. <https://doi.org/10.1098/rstb.2015.0387>.
- [25] Ortega-Jimenez, V. M., and Sanford, C. P., “Beyond the Kármán gait: knifefish swimming in periodic and irregular vortex streets,” *Journal of Experimental Biology*, Vol. 224, No. 10, 2021. <https://doi.org/10.1242/jeb.238808>.
- [26] Gopalkrishnan, R., Triantafyllou, M. S., Triantafyllou, G. S., and Barrett, D., “Active vorticity control in a shear flow using a flapping foil,” *Journal of Fluid Mechanics*, Vol. 274, 1994, pp. 1–21. <https://doi.org/10.1017/S00222112094002016>.
- [27] Liao, J. C., Beal, D. N., Lauder, G. V., and Triantafyllou, M. S., “The Kármán gait: novel body kinematics of rainbow trout swimming in a vortex street,” *Journal of experimental biology*, Vol. 206, No. 6, 2003, pp. 1059–1073. <https://doi.org/10.1242/jeb.00209>.
- [28] Liao, Q., Dong, G.-J., and Lu, X.-Y., “Vortex formation and force characteristics of a foil in the wake of a circular cylinder,” *Journal of fluids and structures*, Vol. 19, No. 4, 2004, pp. 491–510. <https://doi.org/10.1016/j.jfluidstructs.2004.03.001>.

- [29] Chao, L.-M., Zhang, D., Cao, Y.-H., and Pan, G., “Numerical studies on the interaction between two parallel D-cylinder and oscillated foil,” *Modern Physics Letters B*, Vol. 32, No. 06, 2018, p. 1850034. <https://doi.org/10.1142/S0217984918500343>.
- [30] Xiao, Q., Sun, K., Liu, H., and Hu, J., “Computational study on near wake interaction between undulation body and a D-section cylinder,” *Ocean Engineering*, Vol. 38, No. 4, 2011, pp. 673–683. <https://doi.org/10.1016/j.oceaneng.2010.12.017>.
- [31] Shao, X.-m., and Pan, D.-y., “Hydrodynamics of a flapping foil in the wake of a D-section cylinder,” *Journal of Hydrodynamics, Ser. B*, Vol. 23, No. 4, 2011, pp. 422–430. [https://doi.org/10.1016/S1001-6058\(10\)60132-1](https://doi.org/10.1016/S1001-6058(10)60132-1).
- [32] Shao, X., Pan, D., Deng, J., and Yu, Z., “Hydrodynamic performance of a fishlike undulating foil in the wake of a cylinder,” *Physics of Fluids*, Vol. 22, No. 11, 2010, p. 111903. <https://doi.org/10.1063/1.3504651>.
- [33] Akanyeti, O., and Liao, J. C., “A kinematic model of Kármán gaiting in rainbow trout,” *Journal of Experimental Biology*, Vol. 216, No. 24, 2013, pp. 4666–4677. <https://doi.org/10.1242/jeb.093245>.
- [34] Hoffmann, J. A., “Effects of freestream turbulence on the performance characteristics of an airfoil,” *AIAA journal*, Vol. 29, No. 9, 1991, pp. 1353–1354. <https://doi.org/10.2514/3.10745>.
- [35] Devinant, P., Laverne, T., and Hureau, J., “Experimental study of wind-turbine airfoil aerodynamics in high turbulence,” *Journal of Wind Engineering and Industrial Aerodynamics*, Vol. 90, No. 6, 2002, pp. 689–707. [https://doi.org/10.1016/S0167-6105\(02\)00162-9](https://doi.org/10.1016/S0167-6105(02)00162-9).
- [36] Sicot, C., Devinant, P., Laverne, T., Loyer, S., and Hureau, J., “Experimental study of the effect of turbulence on horizontal axis wind turbine aerodynamics,” *Wind energy*, Vol. 9, No. 4, 2006, pp. 361–370. <https://doi.org/10.1002/we.184>.
- [37] Wang, S., Zhou, Y., Alam, M. M., and Yang, H., “Turbulent intensity and Reynolds number effects on an airfoil at low Reynolds numbers,” *Physics of Fluids*, Vol. 26, No. 11, 2014, p. 115107. <https://doi.org/10.1063/1.4901969>.
- [38] Kay, N. J., Richards, P. J., and Sharma, R. N., “Influence of turbulence on cambered and symmetrical airfoils at low Reynolds numbers,” *AIAA Journal*, Vol. 58, No. 5, 2020, pp. 1913–1925. <https://doi.org/10.2514/1.J058822>.
- [39] Amandolese, X., and Széchényi, E., “Experimental study of the effect of turbulence on a section model blade oscillating in stall,” *Wind Energy: An International Journal for Progress and Applications in Wind Power Conversion Technology*, Vol. 7, No. 4, 2004, pp. 267–282. <https://doi.org/10.1002/we.137>.
- [40] Lefebvre, J. N., and Jones, A. R., “Experimental Investigation of Airfoil Performance in the Wake of a Circular Cylinder,” *AIAA Journal*, Vol. 57, No. 7, 2019, pp. 2808–2818. <https://doi.org/10.2514/1.J057468>.
- [41] Zhang, Z., Wang, Z., and Gursul, I., “Lift Enhancement of a Stationary Wing in a Wake,” *AIAA Journal*, Vol. 58, No. 11, 2020, pp. 4613–4619. <https://doi.org/10.2514/1.J059872>.
- [42] Favier, D., Maresca, C., and Rebont, J., “Dynamic stall due to fluctuations of velocity and incidence,” *AIAA Journal*, Vol. 20, No. 7, 1982, pp. 865–871. <https://doi.org/10.2514/3.51145>.

- [43] Shi, Z.-W., and Ming, X., “Effects of Unsteady Freestream on Aerodynamic Characteristics of a Pitching Delta Wing,” *Journal of Aircraft*, Vol. 45, No. 6, 2008, pp. 2182–2185. <https://doi.org/10.2514/1.38925>.
- [44] Shi, Z., and Ming, X., “Experimental investigation on a pitching motion delta wing in unsteady free stream,” *Modern Physics Letters B*, Vol. 23, No. 03, 2009, pp. 409–412. <https://doi.org/10.1142/S0217984909018527>.
- [45] Gharali, K., and Johnson, D. A., “Dynamic Stall Simulation of a Pitching Airfoil under Unsteady Freestream Velocity,” *Journal of Fluids and Structures*, Vol. 42, 2013, pp. 228–244. <https://doi.org/10.1016/j.jfluidstructs.2013.05.005>.
- [46] Yu, J., Leu, T., and Miao, J.-J., “Investigation of reduced frequency and freestream turbulence effects on dynamic stall of a pitching airfoil,” *Journal of Visualization*, Vol. 20, No. 1, 2017, pp. 31–44. <https://doi.org/10.1007/s12650-016-0366-6>.
- [47] Li, Q., Kamada, Y., Maeda, T., Murata, J., and Nishida, Y., “Effect of turbulent inflows on airfoil performance for a Horizontal Axis Wind Turbine at low Reynolds numbers (Part II: Dynamic pressure measurement),” *Energy*, Vol. 112, 2016, pp. 574–587. <https://doi.org/10.1016/j.energy.2016.06.126>.
- [48] Chen, J. M., and Choa, C.-C., “Freestream disturbance effects on an airfoil pitching at constant rate,” *Journal of aircraft*, Vol. 36, No. 3, 1999, pp. 507–514. <https://doi.org/10.2514/2.2485>.
- [49] Merrill, B. E., and Peet, Y. T., “Effect of impinging wake turbulence on the dynamic stall of a pitching airfoil,” *AIAA journal*, Vol. 55, No. 12, 2017, pp. 4094–4112. <https://doi.org/10.2514/1.J055405>.
- [50] Leu, T. S., Yu, J., Hu, C., Miao, J., Liang, S., Li, J., Cheng, J., and Chen, S., “Experimental study of free stream turbulent effects on dynamic stall of pitching airfoil by using particle image velocimetry,” *Applied Mechanics and Materials*, Vol. 225, Trans Tech Publ, 2012, pp. 103–108. <https://doi.org/10.4028/www.scientific.net/AMM.225.103>.
- [51] Conger, R. N., and Ramaprian, B., “Pressure measurements on a pitching airfoil in a water channel,” *AIAA journal*, Vol. 32, No. 1, 1994, pp. 108–115. <https://doi.org/10.2514/3.11957>.
- [52] Kay, N. J., Richards, P. J., and Sharma, R. N., “Effect of Turbulence and Sinusoidal Pitching on Low-Reynolds-Number Lift,” *AIAA Journal*, Vol. 58, No. 6, 2020, pp. 2377–2387. <https://doi.org/10.2514/1.J059169>.
- [53] Marras, S., Killen, S. S., Lindström, J., McKenzie, D. J., Steffensen, J. F., and Domenici, P., “Fish swimming in schools save energy regardless of their spatial position,” *Behavioral Ecology and Sociobiology*, Vol. 69, 2015, pp. 219–226. <https://doi.org/10.1007/s00265-014-1834-4>.
- [54] Poudel, N., Yu, M., and Hrynuk, J. T., “Computational Study on the Effects of Unsteady Freestream on an Airfoil Performance at Low Reynolds Numbers,” *AIAA Scitech 2021 Forum*, 2021, p. 0965. <https://doi.org/10.2514/6.2021-0965>.
- [55] Yu, M., Wang, Z., and Liu, Y., “On the Accuracy and Efficiency of Discontinuous Galerkin, Spectral Difference and Correction Procedure via Reconstruction Methods,” *Journal of Computational Physics*, Vol. 259, 2014, pp. 70–95. <https://doi.org/10.1016/j.jcp.2013.11.023>.

- [56] Yu, M. L., and Wang, L., “A high-order flux reconstruction/correction procedure via reconstruction formulation for unsteady incompressible flow on unstructured moving grids,” *Computers & Fluids*, Vol. 139, 2016, pp. 161–173. <https://doi.org/10.1016/j.compfluid.2016.05.028>.
- [57] Wang, L., and Yu, M. L., “An Implicit High-Order Preconditioned Flux Reconstruction Method for Low-Mach-Number Flow Simulation with Dynamic Meshes,” *International Journal for Numerical Methods in Fluids*, Vol. 91, 2019, pp. 348–366. <https://doi.org/10.1002/flid.4759>.
- [58] Poudel, N., Yu, M., and Hryniuk, J. T., “Gust mitigation with an oscillating airfoil at low Reynolds number,” *Physics of Fluids*, Vol. 33, No. 10, 2021, p. 101905. <https://doi.org/10.1063/5.0065234>.
- [59] Yu, M., Wang, Z., and Hu, H., “A High-Order Spectral Difference Method for Unstructured Dynamic Grids,” *Computers & Fluids*, Vol. 48, No. 1, 2011, pp. 84–97. <https://doi.org/10.1016/j.compfluid.2011.03.015>.
- [60] Huynh, H. T., “A flux reconstruction approach to high-order schemes including discontinuous Galerkin methods,” *18th AIAA Computational Fluid Dynamics Conference*, 2007, p. 4079. <https://doi.org/10.2514/6.2007-4079>.
- [61] Wang, Z., and Gao, H., “A unifying lifting collocation penalty formulation including the discontinuous Galerkin, spectral volume/difference methods for conservation laws on mixed grids,” *Journal of Computational Physics*, Vol. 228, No. 21, 2009, pp. 8161–8186. <https://doi.org/10.1016/j.jcp.2009.07.036>.
- [62] Roe, P. L., “Approximate Riemann solvers, parameter vectors, and difference schemes,” *Journal of computational physics*, Vol. 43, No. 2, 1981, pp. 357–372. [https://doi.org/10.1016/0021-9991\(81\)90128-5](https://doi.org/10.1016/0021-9991(81)90128-5).
- [63] Bassi, F., Crivellini, A., Rebay, S., and Savini, M., “Discontinuous Galerkin Solution of the Reynolds-averaged Navier–Stokes and  $k-\omega$  turbulence model equations,” *Computers & Fluids*, Vol. 34, No. 4, 2005, pp. 507–540. <https://doi.org/10.1016/j.compfluid.2003.08.004>.
- [64] Visbal, M. R., “High-Fidelity Simulation of Transitional Flows Past a Plunging Airfoil,” *AIAA journal*, Vol. 47, No. 11, 2009, pp. 2685–2697. <https://doi.org/10.2514/1.43038>.
- [65] Wang, L., and Yu, M., “Comparison of ROW, ESDIRK, and BDF2 for Unsteady Flows with the High-Order Flux Reconstruction Formulation,” *Journal of Scientific Computing*, Vol. 83, 2020, pp. 1–27. <https://doi.org/10.1007/s10915-020-01222-z>.
- [66] Persson, P.-O., Bonet, J., and Peraire, J., “Discontinuous Galerkin Solution of the Navier–Stokes Equations on Deformable Domains,” *Computer Methods in Applied Mechanics and Engineering*, Vol. 198, No. 17-20, 2009, pp. 1585–1595. <https://doi.org/10.1016/j.cma.2009.01.012>.
- [67] Rutgers, M. A., “Forced 2D turbulence: experimental evidence of simultaneous inverse energy and forward enstrophy cascades,” *Physical review letters*, Vol. 81, No. 11, 1998, p. 2244. <https://doi.org/10.1103/PhysRevLett.81.2244>.
- [68] Watkins, S., Milbank, J., Loxton, B. J., and Melbourne, W. H., “Atmospheric Winds and Their Implications for Microair Vehicles,” *AIAA Journal*, Vol. 44, No. 11, 2006, pp. 2591–2600. <https://doi.org/10.2514/1.22670>.

- [69] Hammer, P. R., Visbal, M. R., Naguib, A. M., and Koochesfahani, M. M., “Lift on a steady 2-D symmetric airfoil in viscous uniform shear flow,” *Journal of Fluid Mechanics*, Vol. 837, 2018. <https://doi.org/10.1017/jfm.2017.895>.
- [70] Laitone, E., “Wind tunnel tests of wings at Reynolds numbers below 70 000,” *Experiments in fluids*, Vol. 23, No. 5, 1997, pp. 405–409. <https://doi.org/10.1007/s003480050128>.
- [71] Young, J., and Lai, J. C., “Oscillation frequency and amplitude effects on the wake of a plunging airfoil,” *AIAA journal*, Vol. 42, No. 10, 2004, pp. 2042–2052. <https://doi.org/10.2514/1.5070>.
- [72] Hammer, P. R., “Computational study of the effect of Reynolds number and motion trajectory asymmetry on the aerodynamics of a pitching airfoil at low Reynolds number,” Ph.D. thesis, Michigan State University, 2016.
- [73] Bohl, D. G., and Koochesfahani, M. M., “MTV measurements of the vortical field in the wake of an airfoil oscillating at high reduced frequency,” *Journal of Fluid Mechanics*, Vol. 620, 2009, pp. 63–88. <https://doi.org/10.1017/S0022112008004734>.
- [74] Yu, M., Wang, B., Wang, Z., and Farokhi, S., “Evolution of vortex structures over flapping foils in shear flows and its impact on aerodynamic performance,” *Journal of Fluids and Structures*, Vol. 76, 2018, pp. 116–134. <https://doi.org/10.1016/j.jfluidstructs.2017.09.012>.
- [75] Hammer, P. R., Olson, D. A., Visbal, M. R., Naguib, A. M., and Koochesfahani, M. M., “Joint Computational-Experimental Investigation of Harmonically Pitching Airfoil Aerodynamics in Uniform-Shear Approach Flow,” *AIAA Journal*, Vol. 57, No. 8, 2019, pp. 3290–3298. <https://doi.org/10.2514/1.J058232>.
- [76] Golubev, V., Nguyen, L., and Visbal, M., “High-fidelity simulations of transitional airfoil interacting with upstream vortical structure,” *49th AIAA Aerospace Sciences Meeting Including the New Horizons Forum and Aerospace Exposition*, 2011, p. 394.
- [77] Floryan, D., Van Buren, T., Rowley, C. W., and Smits, A. J., “Scaling the propulsive performance of heaving and pitching foils,” *Journal of Fluid Mechanics*, Vol. 822, 2017, pp. 386–397. <https://doi.org/10.1017/jfm.2017.302>.